Published in final edited form as:

Cell Rep. 2022 October 25; 41(4): 111538. doi:10.1016/j.celrep.2022.111538.

A multienzyme S-nitrosylation cascade regulates cholesterol homeostasis

Colin T. Stomberski[1,2,3], **Nicholas M. Venetos**[1,2,3], **Hua-Lin Zhou**[2,3,4], **Zhaoxia Qian**[3,4], **Bryce R. Collison**[1,3], **Seth J. Field**[2,4], **Richard T. Premont**[2,3,4], **Jonathan S. Stamler**[2,3,4,5,*]

[1]Department of Biochemistry, Case Western Reserve University School of Medicine, Cleveland, OH 44106, USA

[2]Department of Medicine, Case Western Reserve University School of Medicine, Cleveland, OH 44016, USA

[3]Institute for Transformative Molecular Medicine, Case Western Reserve University School of Medicine, Cleveland, OH 44106, USA

[4]Harrington Discovery Institute, University Hospitals Cleveland Medical Center, Cleveland, OH 44016, USA

[5]Lead contact

SUMMARY

Accumulating evidence suggests that protein S-nitrosylation is enzymatically regulated and that specificity in S-nitrosylation derives from dedicated S-nitrosylases and denitrosylases that conjugate and remove S-nitrosothiols, respectively. Here, we report that mice deficient in the protein denitrosylase SCoR2 (S-nitroso-Coenzyme A Reductase 2; AKR1A1) exhibit marked reductions in serum cholesterol due to reduced secretion of the cholesterol-regulating protein PCSK9. SCoR2 associates with endoplasmic reticulum (ER) secretory machinery to control an S-nitrosylation cascade involving ER cargo-selection proteins SAR1 and SURF4, which moonlight as S-nitrosylases. SAR1 acts as a SURF4 nitrosylase and SURF4 as a PCSK9 nitrosylase to inhibit PCSK9 secretion, while SCoR2 counteracts nitrosylase activity by promoting PCSK9 denitrosylation. Inhibition of PCSK9 by an NO-based drug requires nitrosylase activity, and small-molecule inhibition of SCoR2 phenocopies the PCSK9-mediated reductions in cholesterol observed in SCoR2-deficient mice. Our results reveal enzymatic machinery controlling cholesterol levels through S-nitrosylation and suggest a distinct treatment paradigm for cardiovascular disease.

*Correspondence: jonathan.stamler@case.edu.

AUTHOR CONTRIBUTIONS

C.T.S. and J.S.S. designed the study. C.T.S. carried out most of the experiments and analyzed the results. H.-L.Z., N.M.V., and B.R.C. performed some experiments. Z.Q. handled mice. S.J.F. helped aid experimental design. C.T.S., R.T.P., and J.S.S. wrote the manuscript with input from all authors.

DECLARATION OF INTERESTS

J.S.S. and C.T.S. have patents that relate to discoveries herein. J.S.S. is a co-founder of SNO bio, which develops SNO-based technologies, and serves as a consultant and has an equity stake in NNOXX, a company that is developing NO-related technology.

SUPPLEMENTAL INFORMATION

Supplemental information can be found online at https://doi.org/10.1016/j.celrep.2022.111538.

In brief

PCSK9 regulates LDL receptor levels. Stomberski et al. show that depletion of the SCoR2 denitrosylase lowers serum cholesterol by inhibiting liver PCSK9 secretion. SCoR2 acts on the ER by denitrosylating COPII secretory system components, including SAR1A/B and SURF4. They identify SAR1B and SURF4 as nitrosylases targeting PCSK9 to inhibit PCSK9 secretion.

Graphical Abstract

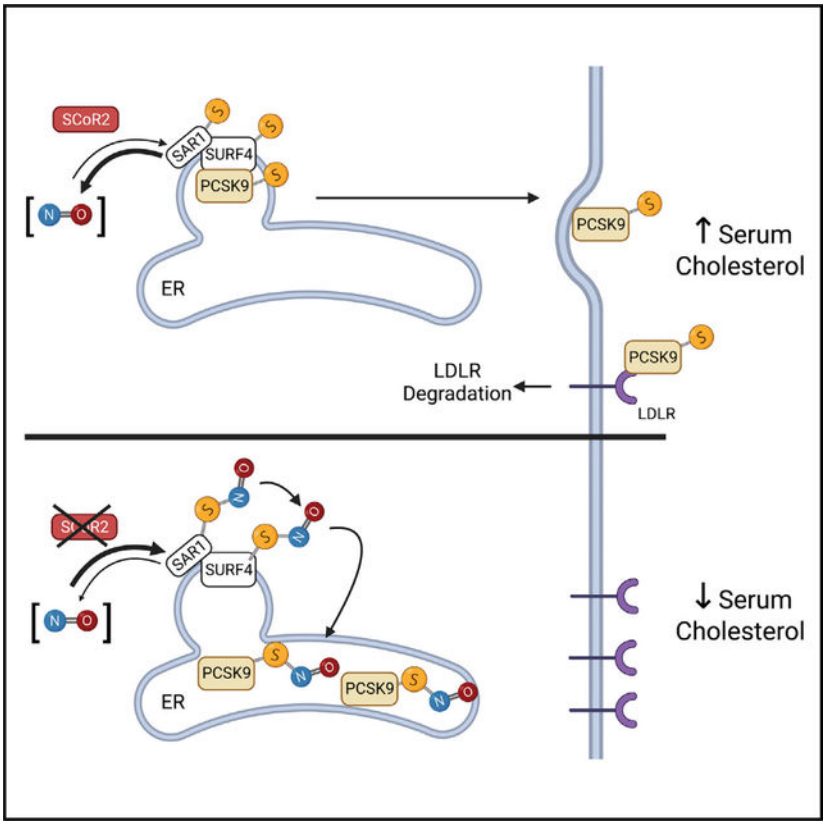

INTRODUCTION

The identification of nitric oxide (NO) as endothelium-derived relaxing factor (Ignarro et al., 1987; Palmer et al., 1987) ushered in the modern era of vascular biology; yet, the medical promise of NO in cardiovascular disease, the most common cause of death in the developed world, remains largely unrealized. While NO bioactivity reduces cardiovascular risk through combined effects on endothelial function, blood pressure, and diabetes (Huang et al., 1995; Johnstone et al., 1993; Kauser et al., 2000; Knowles et al., 2000; Kuhlencordt et al., 2001; Shankar et al., 2000), NO has seemingly little impact on the serum lipoproteins that are primary drivers of the atherogenic process and of disease progression (Knowles et al., 2000; Kuhlencordt et al., 2001; Ozaki et al., 2002). This limitation may help explain why current NO-based drugs do not protect against cardiovascular disease (Nakamura et al., 1999).

NO-mediated regulation of cellular function is achieved primarily through S-nitrosylation, the oxidative modification of Cys thiol by NO to form an S-nitrosothiol (SNO) (Hess et al., 2005). Over 20,000 SNO sites in the literature provide foundation for posttranslational regulation of all main classes of proteins from bacteria to humans (Abunimer et al., 2014; Chen et al., 2010; Li et al., 2021; Seth et al., 2018). Notably, SNOs can be transferred among proteins and other molecules, forming the basis of enzymatic regulation (Jia et al., 2014; Kornberg et al., 2010; Nakamura et al., 2021; Seth et al., 2018; Stomberski et al., 2019a), by direct parallel to enzyme-based group transfer in acetylation, palmitoylation, and ubiquitinylation reactions (Anand and Stamler, 2012; Seth et al., 2018). Coenzyme A (CoA) exemplifies these parallels, as it is used in posttranslational and allosteric regulation of proteins through S-nitroso-CoA (SNO-CoA), palmitoyl-CoA, and acetyl-CoA. In particular, SNO-CoA mediates S-nitrosylation of metabolic proteins (Anand et al., 2014; Stomberski et al., 2019b; Zhou et al., 2019), and CoA-dependent S-nitrosylation is reversed by protein denitrosylases called SNO-CoA reductases (SCoR).

In yeast, a novel SNO-Coenzyme A reductase (SCoR1; *Adh6*) was found to regulate sterol biosynthesis by controlling direct, SNO-CoA-mediated S-nitrosylation of an early sterol synthesis gene (Anand et al., 2014). We therefore considered the possibility that a mammalian counterpart (SCoR2; *AKR1A1*) might play a role in regulating sterol biology. Here we report that mice deficient in SCoR2 exhibit marked reductions in serum cholesterol due instead to inhibitory S-nitrosylation of the cholesterol-regulating protein PCSK9. Notably, we identify a series of protein nitrosylases acting in sequence to inhibit PCSK9 secretion from the endoplasmic reticulum (ER). Inhibition of PCSK9 by an NO-based drug is dependent on nitrosylase activity, and pharmacological inhibition of SCoR2 phenocopies the PCSK9-mediated reduction in cholesterol observed in SCoR2-deficient mice. These results define enzymes controlling cholesterol levels through S-nitrosylation, broaden NO's horizon in reducing cardiovascular risk, and suggest an alternative treatment strategy for cardiovascular disease.

RESULTS

SCoR2$^{-/-}$ mice display LDLR-dependent hypocholesterolemia and low serum PCSK9 levels

Total serum cholesterol was significantly lower in unfasted or fasted (Figures 1A and 1B) mice deficient in the denitrosylase SCoR2 (SCoR2$^{-/-}$) than in wild-type (SCoR2$^{+/+}$) mice, whereas serum triglycerides were unchanged (Figure 1C). Fractionation of pooled serum from SCoR2$^{-/-}$ mice revealed a large reduction in low-density lipoprotein (LDL) cholesterol (~50%) and a smaller reduction in high-density lipoprotein (HDL) cholesterol (~20%) versus SCoR2$^{+/+}$ mice (Figures 1D and 1E).

The liver is central to cholesterol homeostasis (Dietschy and Turley, 2002; Dietschy et al., 1993). SCoR2 is highly expressed in mammalian liver (Stomberski et al., 2019c; Zhou et al., 2019), and SNO-CoA reductase activity is reduced by ~80% in SCoR2$^{-/-}$ livers (Anand et al., 2014). The S-nitrosylation status of key cholesterol homeostatic proteins, including the LDL receptor (SNO-LDLR), HMG-CoA reductase (SNO-HMGCR) and proprotein convertase subtilisin/kexin type 9 (SNO-PCSK9), was assessed by resin assisted capture (SNO-RAC) (Forrester et al., 2009). Notably, each of these proteins was found to be

S-nitrosylated under basal conditions, but only SNO-PCSK9 (catalytic and Cys-His rich domain-containing fragment) levels were elevated in livers from SCoR2$^{-/-}$ mice (Figures 1F and 1G). Further, although the amount of SNO-LDLR was unaltered in SCoR2$^{-/-}$ mice, LDLR protein level was significantly increased (Figures 1F and 1G). By contrast, HMGCR was not different between SCoR2$^{+/+}$ and SCoR2$^{-/-}$ mice (Figures 1F and 1G), nor were SNO or total levels of ACAT2 or ARH (Anand et al., 2014; Zhao et al., 2013), additional proteins involved in cholesterol metabolism (Figures S1A and S1B). Thus, while many cholesterol-regulating proteins are in fact S-nitrosylated in the liver, only SNO-PCSK9 was found to be SCoR2-regulated, and this was associated with increased expression of the LDL receptor.

PCSK9 is a hepatically produced, COPII-secreted (Chen et al., 2013) serum protein that promotes LDL receptor degradation and thus serum LDL accumulation (Horton et al., 2009; Sahng et al., 2004). Genetic variants of PCSK9 influence atherosclerotic risk and cardiovascular outcomes (Burke et al., 2017; Cohen et al., 2005), loss-of-function PCSK9 Cys mutants protect against cardiovascular disease by inhibiting PCSK9 secretion (Cohen et al., 2005; Mayne et al., 2011; Zhao et al., 2006), and antibodies targeting serum PCSK9 are used therapeutically to control hypercholesterolemia (Ge et al., 2021). Indeed, increased amounts of SNO-PCSK9 in SCoR2$^{-/-}$ livers (Figures 1F and 1G) were associated with both increases in hepatic (i.e., intracellular, processed) PCSK9 (Figures 1F–1I) and decreases in serum PCSK9 (Figures 1J and 1K), with no change in PCSK9 mRNA (Figure 1I), consistent with an effect of SNO on PCSK9 secretion. Under these conditions, serum PCSK9 levels and amounts of LDLR should be reciprocally related (through effects on LDLR degradation), which was confirmed in these studies by western blotting in SCoR2$^{+/+}$ vs. SCoR2$^{-/-}$ mice (Figures 1F–1H and 1L) and by unchanged hepatic LDLR mRNA levels (Figure 1L). Moreover, total serum cholesterol was not different between SCoR2$^{+/+}$/LDLR$^{-/-}$ mice and SCoR2$^{-/-}$/LDLR$^{-/-}$ mice (Figure 1M), indicating that LDLR is required for SCoR2-dependent cholesterol lowering. Finally, by contrast with PCSK9, serum levels (and thus secretion) of alpha-1 antitrypsin (another COPII-secreted protein [Emmer et al., 2018]) were not altered by SCoR2 deficiency (Figure S2A), and serum very-low-density-lipoprotein cholesterol was not different between SCoR2$^{+/+}$ and SCoR2$^{-/-}$ mice (Figure 1D). Thus, any effect of SCoR2 on PCSK9 secretion is likely specific to an effect on SNO-PCSK9 (Figures 1F and 1G), and not on secretion generally. Taken together, our results suggest that S-nitrosylation of PCSK9 provides a specific mechanism to reduce serum PCSK9 by inhibiting its secretion throughout the fed/fasted cycle; this stabilizes the hepatic LDLR to enable cholesterol uptake, thereby lowering serum cholesterol.

SCoR2 regulates S-nitrosylation of PCSK9 and its cargo-selection machinery to control PCSK9 secretion

To show directly that the SCoR2/SNO-CoA axis regulates PCSK9 secretion, we generated human hepatoma HepG2 cell lines stably expressing SCoR2-targeting short hairpin RNA (shRNA), and assayed SNO-PCSK9 levels and PCSK9 secretion. Knockdown of SCoR2 in HepG2 cells (Figure S3A) increased amounts of intracellular SNO-PCSK9 (mature fragment) (Figures 2A and 2B) and total PCSK9 (Figures 2C and 2D), while reducing PCSK9 secretion (Figures 2C and 2D). Furthermore, LDLR expression was increased in

SCoR2-depleted HepG2 cells (Figures 2E and 2F). We also generated SCoR2-deficient HEK293 cells (Stomberski et al., 2019b) expressing PCSK9. These cells contained high basal amounts of SNO-PCSK9, and re-expression of SCoR2 reduced SNO-PCSK9 level (Figures 2G and 2H) and increased PCSK9 secretion (Figures 2I and 2J). These results support the notion that denitrosylation of PCSK9 by SCoR2 promotes PCSK9 secretion and, more generally, that SCoR2-regulated S-nitrosylation controls PCSK9 secretion.

Whereas SCoR2 is a cytosolic protein (Barski et al., 2005), PCSK9 undergoes COPII-mediated secretion from within the ER (Chen et al., 2013; Lee et al., 2004), facilitated by the cargo receptor SURF4 (Emmer et al., 2018). Thus, PCSK9 and SCoR2 are compartmentalized away from each other. These data predict involvement of additional SNO-regulatory elements to connect PCSK9 and SCoR2. The COPII coatomer protein is composed of multiple component proteins, including SAR1 (a GTPase with A and B isoforms containing two conserved Cys) and SEC proteins, which form a variety of complexes. In particular, a SAR1A/B–SEC23–SEC24–SURF4 complex has been implicated in cargo selection including PCSK9 (Chen et al., 2013; Emmer et al., 2018), and proximity-labeling studies (Emmer et al., 2018), and other evidence (Wang et al., 2021) suggests that SAR1 and SURF4 cargo receptor interact to regulate lipoprotein metabolism. Indeed, we verified that SAR1B co-immunoprecipitated with SURF4 (Figure S3B) and SURF4 with PCSK9 (*vide infra*), and find that all components of the SAR1A/B–SEC23–SEC24–SURF4 complex are S-nitrosylated and regulated by SCoR2: specifically, amounts of SNO-SAR1A/B and SNO-SURF4, as well as SNO-SEC24A, were reduced dramatically by re-introduction of SCoR2 in SCoR2-deficient HEK293 cells (Figures 2K and 2L). Also, SNO-SAR1A/B and SNO-SEC23A were detected in wild-type mouse livers and levels were greatly elevated in SCoR2$^{-/-}$ livers (Figures 2M and 2N); SNO-SAR1B levels were also elevated in SCoR2 knockdown HepG2 cells (Figures 2O and 2P). In all experiments, expression levels of the proteins themselves, including SAR1A/B, SEC23, SEC24, and SURF4, were unchanged (Figures 2K, 2M, 2O, 2Q–2R). Altogether, these data suggest that SAR1A/B interacts with SURF4, and SURF4 with PCSK9 cargo, and that SCoR2 regulates S-nitrosylation of the COPII coatomer, along with its PCSK9 cargo. Thus, SCoR2-regulated S-nitrosylation may potentially regulate cargo selection.

Transnitrosylation cascade initiated by SAR1A/B regulates PCSK9 S-nitrosylation and secretion

SAR1A/B–SURF4–PCSK9 represent a three-protein complex that effectively spans the cytosol, ER membrane, and ER lumen, respectively. SAR1A/B is cytosolic facing and thus potentially accessible to SCoR2. Thus, we hypothesized that SCoR2 regulates SNO-SAR1A/B in the cytosol and that this SNO-based signal is transmitted across the ER membrane to PCSK9 by SURF4, similar to transduction of SNO bioactivity across red blood cell membranes by AE1/Band 3 (Pawloski et al., 2001). The following *in vitro* complementation assays support this conclusion: immunoprecipitated SAR1B pretreated with S-nitrosocysteine (CySNO) to form SNO-SAR1B, and then incubated (free of CySNO; see methods) with immunoprecipitated SURF4, efficiently nitrosylated SURF4 (Figure 3A). Likewise, immunoprecipitated SURF4 pretreated with CySNO and then incubated with immunoprecipitated PCSK9, efficiently nitrosylated PCSK9 (Figure 3B). Thus, SNO-

SAR1B can transfer SNO to SURF4 and SNO-SURF4 to PCSK9. Together these results suggest a transnitrosylation relay among SAR1A/B–SURF4–PCSK9 where SAR1A/B may act as a SURF4 nitrosylase and SURF4 may act as a PCSK9 nitrosylase.

We verified these findings *in situ* using the cell permeable nitrosylating agent CySNO ethyl ester (ECySNO). Treatment of SCoR2-deficient HEK293 cells with ECySNO increased amounts of SNO-SAR1B and SNO-PCSK9 (Figures 3C and 3D). ECySNO treatment was then repeated in cell lines expressing Cys mutant or wild-type SAR1B ($SAR1B^{C102A/C178A}$ versus $SAR1B^{WT}$). Notably, mutation of cysteines in SAR1B not only abolished SAR1B S-nitrosylation by ECySNO (Figure 3E), but also abolished S-nitrosylation of SURF4 and PCSK9 (Figures 3F and 3G). Furthermore, treatment with ECySNO inhibited PCSK9 secretion in cells expressing $SAR1B^{WT}$ but not in cells expressing $SAR1B^{C102A/C178A}$ (Figures 3H and 3I). Thus, S-nitrosylation of both SURF4 and PCSK9 are dependent on S-nitrosylation of SAR1, and the effect of CySNO to inhibit PCSK9 secretion is dependent on SAR1 S-nitrosylation.

If PCSK9 secretion is inhibited by COPII-mediated S-nitrosylation, then SNO-PCSK9 should be arrested in the ER under the above conditions; also COPII assembly required for transnitrosylation should be unaltered under these conditions. Indeed, ECySNO treatment of SCoR-deficient HEK293 cells stably expressing PCSK9 caused retention of PCSK9 in the ER (Figures 3J and 3K), while the colocalization and assembly of SEC23A/SAR1 (Figures S4A and S4B) were preserved.

SURF4 transnitrosylates PCSK9 to inhibit PCSK9 cargo selection and secretion

A similar set of experiments was performed with SURF4. Treatment of SCoR2-deficient HEK293 cells with ECySNO increased amounts of SNO-SURF4 (Figures 4A and 4B). Among 5 Cys in SURF4, Cys32 is included in the unbiased SNO-proteome database (Chen et al., 2010). SCoR2-deficient HEK293 cell lines expressing wild-type and Cys32-mutant SURF4 ($SURF4^{WT}$ versus $SURF4^{C32A}$) were then treated with ECySNO. Mutation of Cys32 ($SURF4^{C32A}$) not only blunted S-nitrosylation of SURF4 (Figures 4C and 4D), but also prevented S-nitrosylation of PCSK9 (Figures 4D and 4E). Furthermore, treatment with ECySNO reduced PCSK9 secretion in $SURF4^{WT}$ cells but not in $SURF4^{C32A}$ cells (Figures 4F and 4G). Finally, immunoprecipitation of PCSK9 and SURF4 in the presence of ECySNO reduced their interaction (Figures 4H and 4I). Taken together, our results suggest that SNO is relayed through specific Cys residues—from SAR1A/B to SURF4 to PCSK9—to form SNO-PCSK9 and thus inhibit PCSK9 secretion, and that inhibition of PCSK9 secretion by SNO is mediated, at least in part, through diminished interactions between SNO-PCSK9 and SURF4/COPII.

PCSK9 is cleaved during maturation. The cleaved catalytic domain- and Cys-His rich domain (CHRD)-containing fragment of PCSK9 contains 25 Cys residues, and 24 of these are in disulfide bonds and thus not available for nitrosylation in the mature protein (Benjannet et al., 2012; Piper et al., 2007). SNO-PCSK9 levels in mouse livers (Figures 1F and 1G), HepG2 cells (Figures 2A and 2B), and HEK293 cells treated with ECySNO (Figures 3C and 3D) demonstrated consistent dependence on SCoR2, i.e., increased amounts of S-nitrosylation of mature PCSK9 was detected in cells and tissues when SCoR2 was

absent or reduced. We sought to determine the regulatory SNO site on PCSK9. Mass spectrometry analysis of immunoprecipitated and SNO-treated PCSK9 identified Cys255, Cys301, and Cys588 as putative S-nitrosylation sites on PCSK9 (Figures S5A and S5B). Among Cys residues in mature PCSK9, only Cys301 exists as a free thiol (Benjannet et al., 2012; Piper et al., 2007) (Cys255 and Cys588 participate in disulfide bonds). To confirm that Cys301 may act as an allosteric SNO site to mediate the effect of S-nitrosylation on PCSK9 secretion, we transiently expressed $PCSK9^{WT}$ and $PCSK9^{C301A}$ in SCoR2-deficient HEK293 cells. Treatment with ECySNO reduced secretion of $PCSK9^{WT}$ but not $PCSK9^{C301A}$, while secretion of $PCSK9^{C301A}$ was otherwise unaffected by mutation (versus wild-type) (Figures 4J and 4K). Thus S-nitrosylation of PCSK9 at Cys301 is required to inhibit secretion.

Although Cys301 is the only possible S-nitrosylation site in mature PCSK9 protein, mutation of Cys301 did not diminish the SNO-PCSK9 signal (mature fragment; Figures S6A and S6B). These data can be well understood in terms of a role for C301 S-nitrosylation in blocking thiol-disulfide exchange during protein folding and maturation within the ER (Kohr et al., 2011; Murphy et al., 2012; Nagy, 2013), which generates nascent thiol substrate for S-nitrosylation (as in Figure S6A), including C255 and C588. Indeed, when $PCSK9^{WT}$ and $PCSK9^{C301A}$ were separated under non-reducing conditions, the latter showed enhanced disulfides (Figure S6C), albeit without effect on secretion (Figure 4K). Altogether, these results suggest an allosteric role for Cys301 S-nitrosylation in regulating PCSK9 secretion by COPII, involving regulated interactions with cargo-selection proteins, and further suggest a role for Cys301 SNO in quality control of secreted proteins.

Inhibition of SCoR2 by AL-1576 increases SNO-PCSK9 and lowers serum LDL cholesterol

Finally, we sought to determine if pharmacological inhibition of SCoR2 could lower serum cholesterol. AL-1576 is a potent inhibitor of AKR1A1 (SCoR2) (Barski et al., 1995) (whereas other AKR inhibitors trialed clinically do not inhibit AKR1A1). In-diet dosing of AL-1576 for 4 weeks reduced hepatic SCoR2 activity (Figure 5A) to a similar degree as seen in $SCoR2^{-/-}$ mice (Anand et al., 2014). Total serum cholesterol was reduced significantly in AL-1576-treated mice (Figure 5B) and serum fractionation revealed marked reductions in LDL (~50%) and, to a lesser extent, HDL (~20%) cholesterol (Figure 5C), phenocopying SCoR2 deletion (Figure 1). Also consistent with $SCoR2^{-/-}$ mice, AL-1576-treated mice had reduced levels of serum PCSK9 (Figure 5D) and markedly elevated amounts of hepatic SNO-PCSK9 (Figures 5E and 5F); also, serum alpha-1 antitrypsin was not altered by AL-1576 treatment (Figure S2B). Expression analysis in livers from AL-1576-treated mice confirmed expected increases in LDLR and PCSK9 protein levels (Figures 5G and 5H), with no changes in mRNAs for LDLR, PCSK9, or sterolresponse element binding protein 2 (Figure 5I). Further, $LDLR^{-/-}$ mice treated with AL-1576 did not show changes in serum cholesterol (Figure 5J), indicating that LDLR is required for AL-1576-mediated cholesterol reduction. To test the effect of AL-1576 in a more human lipoprotein-relevant mouse model, we used transgenic mice expressing both apoB100 and cholesteryl ester transfer protein (CETP) (Grass et al., 1995). AL-1576 markedly reduced total serum cholesterol in the apoB100/CETP mouse (Figure 5K). Lipoprotein fractionation revealed very large reductions in LDL cholesterol (~70%) with a comparatively modest

lowering of HDL cholesterol (~25%) (Figure 5L). AL-1576 also lowered total and LDL cholesterol in ApoE$^{-/-}$ mice (Figures 5M and 5N) and reduced serum PCSK9 levels (Figure 5O), while hepatic LDLR and PCSK9 levels were both increased (Figures 5P and 5Q). Thus, small molecule inhibition of SCoR2 may represent a distinct mechanism to treat hypercholesterolemia, by augmenting inhibitory S-nitrosylation of PCSK9.

DISCUSSION

Our work describes an unexpected role for S-nitrosylation in lowering serum cholesterol and a first-in-class approach to targeting this pathway therapeutically. S-nitrosylation of the COPII secretory machinery and of cargo protein PCSK9 leads to reductions in PCSK9 secretion and serum levels, thereby lowering serum cholesterol. Specifically, we describe a protein S-nitrosylation cascade that transfers SNOs from cytosol into ER via SAR1A/B–SURF4–PCSK9 to inhibit PCSK9 secretion. The SAR1A/B–SEC23/24–SURF4 complex is involved in cargo selection (Chen et al., 2013; Emmer et al., 2018), and S-nitrosylation of PCSK9 selectively inhibits the SURF4–PCSK9 interaction. Sequential S-nitrosylation of SAR1A/B, SURF4, and PCSK9 is counterbalanced by the protein denitrosylase SCoR2. Inhibition of SCoR2 thus leads to notable increases in SNO-PCSK9 levels *in vivo* (Figure 5E), reduces PCSK9 secretion, and lowers serum cholesterol (Figure 6).

Cholesterol accumulation in the vessel wall is a primary causal factor in millions of deaths annually (Goldstein and Brown, 2015; Virani et al., 2020). While nitric oxide has pleiotropic cardiovascular benefits that reduce atherogenic risk, lowering cholesterol is not traditionally included among these. Nevertheless, we observed profound effects of the SNO-CoA/SCoR2 system on cholesterol homeostasis. This can be understood by appreciating an emerging model in which NO bioactivity is identified with dedicated enzymes that carry out S-nitrosylation (nitrosylases) (Lane et al., 2001; Nakamura et al., 2021; Seth et al., 2018; Stamler and Hess, 2010), and where steady-state levels of S-nitrosylation are determined by cognate enzymes that remove SNOs (denitrosylases) (Stomberski et al., 2019a). In this instance, nitrosylase function is ascribed to both SAR1A/B and SURF4, which are required for S-nitrosylation of SURF4 and PCSK9, respectively. That is, SAR1A/B is a SURF4 nitrosylase and SURF4 a PCSK9 nitrosylase. Further, these S-nitrosylases act within a multienzyme chain that is ultimately regulated by the denitrosylase SCoR2; removal of SNO by SCoR2 thus controls coupled equilibria between SNO-SAR1A/B in the cytosol, SNO-SURF4 in or at the ER membrane, and SNO-PCSK9 in the ER (Figure 6). Alternatively stated, SCoR2 leads to the denitrosylation of SAR1A/B and SURF4 to prevent S-nitrosylation of PCSK9, enabling its secretion. Thus, it would appear that NO has broader purview in cardioprotection than originally thought, including not only canonical effects on blood pressure, diabetes, and endothelial function (Huang et al., 1995; Johnstone et al., 1993; Kauser et al., 2000; Knowles et al., 2000; Kuhlencordt et al., 2001; Shankar et al., 2000), but also via cholesterol regulation.

Our model highlights directions for future work. Foremost among these is the likely role that S-nitrosylation of COPII component proteins may play in coordinating ER secretion, independent of PCSK9 nitrosylation. For example, S-nitrosylation of the Ras GTPase enhances its function (Huang et al., 2014), but functional effects on SAR1A/B are

unexplored. Second, tenets of diffusion of NO across membranes (Lancaster, 1994) would appear overly simplified. In particular, we find an SNO cascade across the ER membrane using SURF4, which incomplete as it is, finds precedent in the cysteine-to-cysteine trans-membrane transfer of SNO out of erythrocytes by AE1/Band 3 (Hongoh et al., 2012; Pawloski et al., 2001). Finally, the mechanisms that allow proteins to transfer SNO in a specific manner (Seth et al., 2018) represents an emerging area of research. It is clear, nonetheless, that protein-protein interactions are needed to stabilize SNO donor and target Cys residue orientations to allow transfer (Houk et al., 2003; Seth et al., 2018; Stomberski et al., 2019a), and reader motifs may be required as well (Jia et al., 2014; Marino and Gladyshev, 2010). One related finding of great surprise is that the NO donor CySNO, which has long been assumed to S-nitrosylate proteins such as PCSK9 indiscriminately, is shown here to depend on nitrosylases for its action. That is, NO donors may not mediate S-nitrosylation directly, but instead may provide substrate for nitrosylases (Seth et al., 2018), potentially changing interpretation of a large literature.

These considerations notwithstanding, the SNO relay between Cys102/178 in SAR1A/B, Cys32 in SURF4, and Cys301 in PCSK9 serves in signal transduction (between cytosol and ER) on the one hand, and to confer specificity on PCSK9 secretion, on the other hand. Once S-nitrosylated, PCSK9's interaction with its direct nitrosylase and ER cargo receptor SURF4 is inhibited, presumably leaving this ER cargo receptor available for its other substrates. PCSK9 secretion is also inhibited without affecting secretion of SURF4-independent proteins such as alpha-1 antitrypsin. Interestingly, serine phosphorylation is proposed to activate PCSK9 (Ben Djoudi Ouadda et al., 2019) and promote LDLR degradation, suggesting crosstalk with S-nitrosylation to regulate PCSK9 activity. As with phosphorylation, S-nitrosylation may be targeted for therapeutic gain. Small-molecule inhibition of SCoR2 has a powerful cholesterol-lowering effect suggesting therapeutic benefit (Figures 5B, 5C, 5K–5N) as seen with anti-PCSK9 antibody therapy (Ge et al., 2021). SNO-regulatory enzymes may thus provide distinct access into human disease.

Limitations of the study

First, while we have provided both genetic and biochemical evidence that SNO-based modification of PCSK9 controls its secretion, we do not exclude roles for other electrophilic modifications in PCSK9 physiology. Second, technical limitations, including lack of robust antibodies for SURF and SNOs, precluded the assessment of SNO-SURF4 in murine liver and accurate subcellular localization of SNO-PCSK9. Also, SNO-RAC based methodology may occasionally detect alternative electrophilic modifications if all control steps are not routinely performed (Forrester et al., 2007). Third, the precise mechanism by which SNO transits the ER membrane via SURF4 on the one hand, and a broader role for S-nitrosylation in COPII function and ER cargo recognition, on the other hand, remain to be studied. Finally, further work should consider the effect of SCoR2 in atherosclerosis models to confirm the importance of cholesterol versus cellular mechanisms in disease pathogenesis.

STAR★METHODS

RESOURCE AVAILABILITY

Lead contact—Further information and request for resources and reagents should be directed to and will be fulfilled by the lead contact, Jonathan Stamler (jonathan.stamler@case.edu).

Materials availability—All newly generated plasmids and cells lines are available upon request to the lead contact. The distribution of reagents will be subject to a MTA.

Data and code availability

- Original western blot images and microscopy images are available publically on Mendeley Data at the DOI listed in the key resources table. Mass spectrometry data will be shared by the lead contact upon request.
- This paper does not report original code.
- Any additional information required to reanalyze the data reported in this paper is available from the lead contact by request.

EXPERIMENTAL MODEL AND SUBJECT DETAILS

Animals—Mouse studies were approved by the Institutional Animal Care and Use Committee (IACUC) at Case Western Reserve University. All housing and procedures complied with the *Guide for the Care and Use of Laboratory Animals* and the American Veterinary Medical Association Guidelines regarding euthanasia. Generation of *SCoR2*$^{-/-}$ mice was described previously (Anand et al., 2014). C57BL/6J, *LDLR*$^{-/-}$, and ApoE$^{-/-}$ mice were purchased from Jackson Laboratory. CETP-ApoB100 transgenic mice were purchased from Taconic. To generate SCoR2 and LDLR double knockout mice, *SCoR2*$^{-/-}$ male mice were initially bred to LDLR$^{-/-}$ female mice. Resulting compound heterozygotes were bred to generate SCoR2$^{+/-}$/LDLR$^{-/-}$ females and SCoR2$^{-/-}$/LDLR$^{-/-}$ males, which were subsequently bred together to propagate SCoR2$^{-/-}$/LDLR$^{-/-}$ males for experimental use. All mice were maintained on a 12-h light/dark cycle with standard housing and husbandry. For all studies, male mice between ages 10–20 weeks were used as specified for each experiment in figure legends. Age-matched male controls were selected from littermates. For drug treatment studies, age-matched male littermates were randomly assigned to treatment groups. All animals were treatment and procedure naive at the time of allocation to specific studies. Genotyping was performed by standard methods using the primers listed in Table S1.

Beginning at 8 weeks of age, any *SCoR2*$^{-/-}$ mice were fed AIN-93M mature rodent diet (Research Diets) supplemented with 1% ascorbic acid to overcome their inability to synthesize ascorbic acid; *SCoR2*$^{+/+}$ mice were fed AIN-93M.

Cell lines—HepG2 and 293T/17 cells were obtained from ATCC and cultured at 37°C, 5% CO_2 in growth media [DMEM (Gibco) supplemented with 10% fetal bovine serum (Sigma), 1X antibiotic-antimycotic (Gibco), and 1X GlutaMax (Gibco)]. SCoR2-knockout

HEK293 were described previously (Stomberski et al., 2019b) and were cultured at 37°C, 5% CO_2 in growth media. SCoR2-knockout HEK293 cells stably expressing PCSK9 were cultured at 37°C, 5% CO_2 in growth media supplemented with 200 μg/mL Geneticin (Gibco). HepG2 cells stably expressing SCoR2-targeting shRNA or non-targeting shRNA were cultured in growth media supplemented with 2μg/mL puromycin (Gibco). Cell lines were not authenticated.

METHOD DETAILS

Experimental drug treatment—For AL-1576 treatment studies, C57BL/6J, CETP-ApoB100 transgenic, and $LDLR^{-/-}$ mice were fed control diet (AIN-93M) or experimental diet (AIN-93M supplemented with 0.0125% AL-1576) for indicated lengths of time.

Mouse euthanasia and sample collection—For serum and tissue collection, mice were anesthetized with isoflurane and euthanized by terminal exsanguination and removal of vital organs. Tissues were snap frozen in liquid nitrogen and stored at −80°C until analysis. Blood was transferred to serum separator tubes (BD Microtainer, 365967) and allowed to coagulate for 20 min at room temperature. Serum was separated by centrifugation at 2000g for 15 min at 4°C and stored at −80°C until analysis.

Serum chemistries—Total serum cholesterol and serum triglycerides were measured by standard enzymatic methods. For 12-week old $SCoR2^{+/+}$ and $SCoR2^{-/-}$ mice, serum cholesterol and serum triglycerides were measured at University Hospitals Cleveland Medical Center Clinical Laboratory. Lipoprotein fractionation was performed by the Vanderbilt University Medical Center Lipid Lab. Briefly, lipoprotein fractions were separated from 0.1 mL of serum (pooled from the indicated number of mice for each test group) by gel filtration column chromatography. Approximately 70 fractions (0.25 mL) are collected and the amount of cholesterol in each fraction is determined using microtiter plate enzyme-based assays. Cholesterol profiles are constructed and calibration of the column with purified lipoprotein fractions permits quantitation of cholesterol in various lipoprotein classes. Serum PCSK9 was measured using the PCSK9 Quantikine ELISA kit following manufacturer's instructions. Serum alpha-1 antitrypsin was measured using the alpha-1 antitrypsin ELISA kit following manufacturer's instructions.

Immunoblotting—Immunoblotting analysis was performed by standard procedures under reducing conditions (unless otherwise specified) on proteins extracted from tissues or cells as described below. Antibodies used are listed in the key resources table. All blots were quantified using ImageJ (NIH).

Mouse tissue analysis by immunoblotting and quantitative reverse transcription PCR—For mouse tissue protein analysis, frozen liver tissue was lysed by mechanical homogenization in RIPA buffer (5–10 μL lysis buffer/1 mg tissue; Alfa Aesar, J62524) containing protease inhibitors (Roche, 04693159001). Lysate was clarified by centrifugation (20000g, 4°C, 30 min, X2) and protein concentration determined by the bicinchoninic acid (BCA) method. Proteins were analyzed by SDS-PAGE and immunoblotting.

For SNO-protein analysis in mouse livers, SNO-RAC was performed as described previously (Forrester et al., 2009), as follows. Frozen liver tissue was lysed by mechanical homogenization in HEN buffer (100 mM HEPES, 1 mM EDTA, 0.1 mM neocuproine, pH 8.0) with 150 mM NaCl, 1% Nonidet P-40 (NP-40), 0.1% S-methylmethanethiosulfonate (MMTS) and protease inhibitors. Lysate was clarified by centrifugation (20,000g, 4°C, 30 min, twice) and protein determined by BCA method. 4 mg of protein was added to HEN buffer containing 2.5% SDS and 0.2% MMTS and incubated at 50°C for 20 min with frequent vortexing. Proteins were precipitated with ice cold acetone and re-dissolved in HEN buffer with 1% SDS (HENS). Protein precipitation and resuspension was repeated once and protein concentration estimated by BCA assay. 1–2 mg (equal amounts per sample) of protein was incubated 50 μL of thiopropyl-Sepharose 6B (50% bead slurry, GE Healthcare) in the presence or absence of 30mM ascorbate for 3–4 h with rotation in the dark. Protein-bound beads were washed 4 times with 1 mL of HENS buffer and 2 times with 1 mL of HENS buffer diluted 1/10 with MilliQ grade water. SNO-proteins were eluted in 2X loading dye containing 10% β-mercaptoethanol, separated by SDS-PAGE, and analyzed by immunoblotting.

For mouse mRNA analysis, mRNA was isolated from frozen liver tissue using RNeasy mini prep kit (Qiagen, 74104) following manufacturer's instructions. RNA was quantified using a NanoDrop microvolume spectrophotometer (Thermo). 1 μg of RNA was converted to cDNA using High-Capacity RNA-to-cDNA kit. Quantitative PCR was performed on Applied Biosystems OneStepPlus system using TaqMan Universal Master Mix II (without UNG). Briefly, 10 μL of TaqMan Universal Master Mix II, 1 μL of TaqMan Assay probe (listed below for each gene), 1 μL of cDNA product, and 8 μL of DNase/RNase free water was combined for each reaction. Reactions were performed in triplicate for each sample using the following program: 10 min at 95°C followed by 40 cycles of 15 s at 95°C and 1 min at 60°C. Data were analyzed using the comparative C_T method. TaqMan Assay probes (Thermo) are listed in the key resources table.

Expression plasmids—The PCSK9 coding sequence in pEntr223.1 (Dharmacon) was shuttled to pcDNA-DEST40 vector using LR Clonase II (Thermo Fisher, 11791100) per manufacturer's instructions and verified by sequencing. $PCSK9^{C301A}$ was generated by site-directed mutagenesis of pcDNA-DEST40-$PCSK9^{WT}$ using the Agilent QuikChange XL II system per manufacturer's instructions. The mutagenesis primers are listed in Table S2. Mutation was verified by sequencing. An additional PCSK9-FLAG construct was generated by shuttling PCSK9 coding sequence in pEntr223.1 (DNASU) to pCSF107mT-GATEWAY-3'-FLAG as above. Successful FLAG-tagging was assessed by sequencing and immunoblotting.

N-terminal V5-tagged SURF4 expression plasmid was generated as follows. Human SURF4 cDNA in pDONR221 vector was shuttled to pcDNA3.2/nV5-DEST vector using Gateway LR Clonase II enzyme mix per manufacturer's instructions. Successful clones were validated by sequencing and immunoblotting. SURF4 mutants were generated by site-directed mutagenesis of SURF4 expression vector using the Agilent QuikChange XL II system per manufacturer's instructions. Mutagenesis primers are listed in Table S2. Mutation was verified by sequencing.

SAR1B expression plasmid and AKR1A1/SCoR2 expression plasmid were purchased from Origene. SAR1B mutants were generated by site-directed mutagenesis of SAR1B expression vector using the Agilent QuikChange XL II system per manufacturer's instructions. Mutagenesis primers are listed in Table S2. $SAR1B^{C102A/C178A}$ was generated sequentially. Mutation was verified by sequencing.

Generation of HepG2 stably expressing SCoR2-targeting shRNA—HepG2 cells stably expressing SCoR2-targeting shRNA were produced as follows. 293T/17 cells were plated on 6-well plates and transfected with either mammalian non-targeting Mission shRNA or SCoR2-targeting Mission shRNA in combination with Mission Lentiviral packaging mix (Sigma, SHP001) using PolyJet transfection reagent (SignaGen, SL100688) per manufacturers' instructions. After 24 h, media was aspirated from cells and 2 mL of fresh growth media was applied. After 24 h, 2 mL of media containing lentivirus was collected and stored at 4°C overnight. Viral media production was repeated. The resulting 4 mL of viral media was centrifuged to remove any cells and 3.5 mL of media retained. 1.5 mL of growth media was added to bring the final volume to 5 mL of viral media. 4 μL of 10 mg/mL polybrene (Sigma, TR-1003) was added to media to a final concentration of 8 μg/mL. The viral supernatant was applied to HepG2 cells and allowed to incubate for 6 h. After 6 h, 10 mL of growth media was added to the viral media and cells were incubated for 72 h. After 72 h, HepG2 cells were split into growth media supplemented with 2 μg/mL puromycin (Gibco) and cultured consecutively to select for shRNA expressing cells. SCoR2 knockdown was confirmed by immunoblotting.

Cell-based PCSK9 secretion assays and SNO-protein analysis—PCSK9 secretion assays in HepG2 cells were performed as follows. Equal numbers of $HepG2^{shCtrl}$ and $HepG2^{shSCoR2}$ cells were plated onto dishes coated with 5 μg/cm^2 rat tail collagen I (Corning) and cultured for 24 h. After 24 h, growth media containing 2 μg/mL puromycin was removed from cells and replaced with plain Opti-MEM media (Gibco) supplemented with 1.5 μg/mL puromycin. Cells were cultured for another 24 h and then washed twice with warm PBS. Fresh Opti-MEM (with 1.5 μg/mL puromycin and lacking PCSK9) was added to cells and cells were incubated for 3 h at 37°C, 5% CO_2. After 3 h, media was collected and centrifuged to pellet any cellular material. Cells were washed 3 times with cold PBS and harvested in RIPA buffer containing protease inhibitors (Roche). Cells were lysed by brief sonication, cell debris pelleted by centrifugation (12,000g, 4°C, 10 min), and protein concentration determined by BCA assay. Proteins were separated by SDS-PAGE and analyzed by immunoblotting. For media PCSK9 analysis, equal volumes of media were separated by SDS-PAGE and analyzed by immunoblotting.

For SNO-protein analysis in $HepG2^{shCtrl}$ and $HepG2^{shSCoR2}$ cells, equal numbers of $HepG2^{shCtrl}$ and $HepG2^{shSCoR2}$ were plated onto dishes coated with 5 μg/mL rat tail collagen I (Corning) and cultured for 24 h. After 24 h, growth media containing 2 μg/mL puromycin was removed from cells and replaced with plain Opti-MEM media (Gibco) supplemented with 1.5 μg/mL puromycin. Cells were cultured for another 24 h and harvested in HEN buffer with 150 mM NaCl, 1% Nonidet P-40 (NP-40), 0.1% S-methylmethanethiosulfonate (MMTS) and protease inhibitors (Roche). Cells were lysed

by brief sonication and cell debris pelleted by centrifugation (12,000g, 4°C, 10 min). The entire cell lysate was brought to 2 mL with HEN buffer and 2.5% SDS and 0.2% MMTS was added. Lysate incubated at 50°C for 20 min with frequent vortexing. Proteins were precipitated with ice cold acetone and re-dissolved in HEN buffer with 1% SDS (HENS). Protein precipitation and resuspension was repeated once and protein concentration estimated by BCA assay. 1 mg of protein was incubated with 50 μL of thiopropyl-Sepharose (50% bead slurry) in the presence or absence of 30mM ascorbate for 3–4 h with rotation in the dark. Protein-bound beads were washed 4 times with 1 mL of HENS buffer and 2 times with 1 mL of HENS buffer diluted 1/10 with MilliQ grade water. SNO-proteins were eluted in 2X loading dye containing 10% β-mercaptoethanol, separated by SDS-PAGE, and analyzed by immunoblotting.

For PCSK9 secretion assays and SNO-RAC analysis in SCoR2-deficient HEK293, equal numbers of SCoR2 knockout HEK293 cells were plated onto dishes coated with 5 μg/cm^2 poly-D-lysine (Corning) and cultured for 24 h in growth media. Cells were transfected with indicated wild-type or mutant expression plasmids using PolyJet transfection reagent per manufacturer's instructions. After 24 h, cells were washed twice with warm PBS and an equal volume of plain Opti-MEM. 1M Ethyl ester SNO-cysteine (ECySNO) was freshly prepared by mixing equal volumes of 2M sodium nitrite with 2M acidified ethyl ester cysteine (0.5M HCl) to generate 1M ECySNO. ECySNO was immediately added to designated cells at a final concentration of 200 μM or as otherwise indicated. After 90 min, media was collected and centrifuged to pellet any cellular material. Cells were washed 3 times with cold PBS and harvested in HEN buffer with 150 mM NaCl, 1% Nonidet P-40 (NP-40), 0.1% S-methylmethanethiosulfonate (MMTS) and protease inhibitors (Roche). Cells were lysed by brief sonication, cell debris pelleted by centrifugation (12,000g, 4°C, 10 min), and protein concentration determined by BCA assay. SNO-protein analysis was performed as described above. Otherwise, proteins were separated by SDS-PAGE and analyzed by immunoblotting. For media PCSK9 analysis, equal volumes of media were separated by SDS-PAGE and analyzed by immunoblotting. For non-reducing conditions, protein samples were prepared for SDS-PAGE without the addition of β-mercaptoethanol in loading buffer.

Co-immunoprecipitation—Co-immunoprecipitation of SURF4 and PCSK9 was performed as follows. Equal numbers of SCoR2 knockout HEK293 cells were plated for overnight growth. Cells were transfected with indicated combinations of PCSK9^{WT} and V5-SURF4 expression vectors using PolyJet transfection reagent (SignaGen) per manufacturer's instructions and grown for 24 h. Cells were washed with warm PBS and media replaced with Opti-MEM media with or without 200 μM ECySNO for 20 min prior to harvest. After incubation, cells were washed 2X with room temperature PBS containing 2mM $CaCl_2$. Cells were harvested by scraping into PBS containing 2 mM $CaCl_2$ and pelleted at 1400 RPM for 3 min at room temperature. Supernatant was removed and cells were resuspended in PBS containing 2 mM $CaCl_2$ and 2 mM dithiobis(succinimidyl propionate). Cells were rotated for 30 min at room temperature. The crosslinking reaction was quenched by the addition of 1M Tris buffer, pH 7.4 to a final concentration of 25 mM Tris buffer and rotated for an additional 15 min. Cells were pelleted at 1400 RPM for 3 min and

supernatant removed. Cells were lysed by sonication in RIPA buffer containing protease inhibitor cocktail (Roche). Cell debris was pelleted at 12,000g for 10 min at 4°C. Anti-V5 agarose affinity gel was equilibrated into RIPA buffer and clarified lysate was applied to the anti-V5 agarose affinity gel. Lysate/gel suspension was rotated for 90 min at room temperature. Following rotation, beads were washed 4 times with room temperature RIPA buffer. Proteins were eluted by shaking beads for 30 min at room temperature in 2x Laemmli sample buffer containing 10% β-mercaptoethanol. Proteins were separated by SDS-PAGE and analyzed by immunoblotting. Note that samples containing SURF4 were not boiled at any stage during sample preparation; we find that boiling leads to significant aggregation of SURF4.

Co-immunoprecipitation of SAR1B and SURF4 was performed as follows. Equal numbers of 293T/17 cells were plated for overnight growth. Cells were transfected with indicated combinations of SAR1B-FLAG and V5-SURF4 expression vectors using PolyJet transfection reagent per manufacturer's instructions and grown for 24 h. Cells were harvested in IP wash buffer (50 mM Tris buffer pH 7.4, 150 mM NaCl, 1 mM EDTA, 0.1% NP-40) supplemented with 0.5% Triton X-100 and protease inhibitor cocktail (Roche) and cells were lysed by sonication. Cell debris was pelleted at 15000g for 15 min. Anti-V5 agarose affinity gel was equilibrated into IP wash buffer and clarified lysate was applied to the anti-V5 agarose affinity gel. Lysate/gel suspension was rotated for 120 min at room temperature. Following rotation, beads were washed 4 times with room temperature IP wash buffer. Proteins were eluted in IP wash buffer containing 500 μg/mL V5 peptide with shaking at room temperature for 30 min. Eluted protein was mixed with 4X loading dye containing 10% β-mercaptoethanol. Proteins were separated by SDS-PAGE and analyzed by immunoblotting.

Transnitrosylation assay—Transnitrosylation assays (SAR1B-FLAG to V5-SURF4 and V5-SURF4 to PCSK9-FLAG) were performed as follows using the stated combinations. Equal numbers of 293T/17 cells were plated for overnight growth. The following day, cells were transfected with indicated constructs using PolyJet transfection reagent (SignaGen) per manufacturer's instructions and grown for 24 h. After 24 h, cells were harvested in IP wash buffer (as above) supplemented with 0.5% Triton X-100 and protease inhibitor cocktail (Roche). Cells were lysed by sonication and lysate clarified by centrifugation at 15000g for 15 min. Anti-V5 agarose affinity gel and anti-FLAG agarose affinity gel were equilibrated into IP wash buffer and clarified lysate was applied to the anti-V5 agarose affinity gel or anti-FLAG agarose affinity gel depending on protein tag. Lysate/gel suspension was rotated for 120 min at room temperature. Following rotation, beads were washed 4 times with room temperature IP wash buffer. Proteins were eluted in 300 μL IP wash buffer containing 500 μg/mL V5 peptide or 500 μg/mL 3X FLAG peptide with shaking at room temperature for 30 min 250 μL of supernatant was collected and stored at 4°C overnight without protection from light. S-nitrosylation reactions were performed as follows. 100 μL of immunoprecipitated transnitrosylation donor protein (SAR1B or SURF4) was added to 400 μL assay buffer (phosphate buffer pH 7.0 supplemented with 100 μM EDTA and DTPA and 0.1% NP-40). Two tubes were prepared. A third tube containing 500 μL assay buffer was prepared. 2 μL of freshly prepared 250 mM S-nitroso-cysteine (CySNO) was added to

one tube containing the donor transnitrosylase protein (SNO-donor protein) and to the tube containing only assay buffer (control reaction). All 3 tubes were incubated for 30 min at 37°C. Following incubation, the three reaction mixtures and a fourth tube containing 200 μL of immunoprecipitated transnitrosylation target protein (SURF4 or PCSK9) and 300 μL of assay buffer were concentrated at 14000g for 10 min through a 10 kDa cutoff filter pre-equilibrated with assay buffer (removing CySNO). Buffer exchange was performed 4 additional times, with the final spin lasting for 5 min. Following washes, transnitrosylation reactions were set up as follows: i) 30 μL CySNO-treated buffer without donor protein +10 μL target protein +260 μL assay buffer; ii) 30 μL CySNO-treated donor protein +10 μL target protein +260 μL assay buffer; iii) 30 μL untreated donor protein +10 μL target protein +260 μL assay buffer. Reactions were incubated at 37°C for 30 min in the dark. Reactions were quenched by the addition of 3 volumes ice cold 100% acetone. Following quenching, 25 μL of 2 μg/μL BSA was added to samples. Proteins were precipitated at −20°C for 30 min, pelleted at 4500g for 8 min, and washed 4X with 70% acetone. Protein pellets were resuspended in 300 μL HEN buffer containing 2.5% SDS and 0.3% MMTS. Resuspended proteins were processed by SNO-RAC as described above.

Generation of HEK293 stably expressing PCSK9—HEK-293 cells stably expressing PCSK9 were produced as follows. HEK-293 cells were transfected with pcDNA-DEST40-$PCSK9^{WT}$ using PolyJet transfection reagent per manufacturer's instructions. 16 h after transfection, media was replaced and cells were grown to ~90% confluency. Cells were then split into growth media containing 200 μg/mL Geneticin to select for PCSK9-expressing cells. Expression was confirmed by western blot.

Immunofluorescence—Cells were grown on collagen-coated 12-mm coverslips and fixed with 4% paraformaldehyde. Fixed cells were permeabilized with 0.05% Triton X-100 in PBS and blocked with 8% BSA in PBS. For PCSK9 visualization experiments, cells were stained with rabbit PCSK9 primary (Proteintech) and mouse Calnexin primary then stained with Alexa488-conjugated anti-rabbit and Alexa594-conjugated anti-mouse secondary antibodies. For Sec23A and Sar1B colocalization experiments, cells were stained with rabbit Sar1B primary (Abcam) and goat Sec23A primary (Novus Biologicals) then stained with Alexa488-conjugated anti-rabbit and Alexa594-conjugated anti-goat secondary antibodies. All fluorescence microscopy was performed using an Andor Dragonfly spinning disk confocal microscope system, on a Nikon Ti2 using a 60x/1.4 NA objective lens. Illumination was provided by 488nm and 561nm wavelength solid state diode lasers, illumination field homogenized using Borealis Laser Light Source, and images captured with a Zyla Plus sCMOS camera. Acquisition was performed using Fusion software. All analysis was performed in ImageJ software and colocalization was performed using the JACoP plugin. For Sec23A and Sar1B colocalization experiments, images were adjusted to similar intensities within ImarisViewer before analysis in ImageJ.

Identification of PCSK9 SNO site by mass spectrometry—PCSK9-FLAG was overexpressed in HEK293 cells using PolyJet (as above). Cells were harvested and lysed in EBC lysis buffer. PCSK9-FLAG was purified from lysate with anti-FLAG M2 affinity gel and eluted from the affinity gel with 100 mM phosphate buffer, pH 7.4 containing

100 μg/mL FLAG peptide, 100 μM EDTA and 100 μM DTPA. Purified PCSK9 was subsequently treated with 100 μM freshly prepared SNO-CoA for 20 minutes at room temperature in a dark room.

Following treatment with SNO-CoA, protein was precipitated with 100μg bovine serum albumin using 3 volumes ice cold 100% acetone and kept at −20°C for 20 min. Following cold incubation, precipitated protein was spun at 14000g for 15 min. Pelleted protein was washed 3 times with ice cold 70% acetone. Pelleted protein was resuspended in HENS buffer. Unreacted SNO-CoA was removed using Zeba desalting spin columns (Thermo Fisher) preequilibrated with HENS buffer. Following filtration, 20 μL of 1M MMTS was added to the protein solution and the solution was vortexed. The solution was incubated for 30 min at RT to block free thiols. Protein was again precipitated with 3 volumes ice cold 100% acetone and incubated for 1 h at −20°C. Following incubation, precipitated proteins were centrifuged at 10000g for 10 min at 4°C. Supernatant was removed from precipitated protein pellets, and pellets were allowed to dry at room temperature for 10 min. Proteins were resuspended in HENS buffer and labeled with iodoTMT (Thermo Fisher) in the presence of 20 mM sodium ascorbate for 1 h at room temperature in the dark. Reactions were quenched with 20 mM DTT for 15 min at room temperature in the dark. Protein was precipitated with 3 volumes ice cold 100% acetone at −20°C for 1 h, then centrifuged at 10000g for 10 min at 4°C. Supernatant was removed and protein pellet dried for 10 min. Protein was resuspended in HENS buffer and treated with 16.67 mM iodoacetamide for 1 h at room temperature in the dark. Protein was again precipitated as above, supernatant removed, and protein pellet dried.

Precipitated protein was then resuspended in 50 mM ammonium bicarbonate buffer, pH 8.0. Proteins were then serially digested with 25 μg/mg protein of Lys-c (4 h at 37°C) then 20 μg/mg protein of trypsin overnight at 37°C. Following digestion, samples were acidified with 25 μL of 10% TFA. Peptides were processed through a C18 SPE column and then frozen and lyophilized.

Lyophilized peptides were resuspended in TBS and enriched with anti-TMT resin (Thermo Fisher) following manufacturer's instructions and subsequently frozen and lyophilized. Samples were resuspended in 5% acetonitrile, 0.1% formic acid and run through a 0.22 μm filter to remove any excess anti-TMT resin. Samples were then injected into LC-MS/MS system for analysis.

QUANTIFICATION AND STATISTICAL ANALYSIS

Statistical analysis was performed when indicated using GraphPad Prism 7 to calculate p values from Student's t-test, one-way ANOVA, and Pearson's coefficient, as applicable to a given study. Figure legends detail the statistical test, exact value of n and what it represents, and dispersion and precision measures for each experiment. Throughout the manuscript, significance was defined as a p value < 0.05.

Supplementary Material

Refer to Web version on PubMed Central for supplementary material.

ACKNOWLEDGMENTS

We thank Precious McLaughlin for help generating experimental tools and the lipid core at the Vanderbilt Mouse Metabolic Phenotyping Core for cholesterol fractionation experiments. Supported by American Heart Association-Allen Brain Health Initiative grant 19PABHI34580006 and NIH grants HL075443, HL128192, HL126900, and DK119506.

REFERENCES

Abunimer A, Smith K, Wu T-J, Lam P, Simonyan V, and Mazumder R (2014). Single-nucleotide variations in cardiac arrhythmias: prospects for genomics and proteomics based biomarker discovery and diagnostics. Genes 5, 254–269. [PubMed: 24705329]

Anand P, and Stamler JS (2012). Enzymatic mechanisms regulating protein S-nitrosylation: implications in health and disease. J. Mol. Med. 90, 233–244. [PubMed: 22361849]

Anand P, Hausladen A, Wang YJ, Zhang GF, Stomberski C, Brunengraber H, Hess DT, and Stamler JS (2014). Identification of S-nitroso-CoA reductases that regulate protein S-nitrosylation. Proc. Natl. Acad. Sci. USA 111, 18572–18577. [PubMed: 25512491]

Barski OA, Gabbay KH, Grimshaw CE, and Bohren KM (1995). Mechanism of human aldehyde reductase: characterization of the active site pocket. Biochemistry 34, 11264–11275. [PubMed: 7669785]

Barski OA, Papusha VZ, Ivanova MM, Rudman DM, and Finegold MJ (2005). Developmental expression and function of aldehyde reductase in proximal tubules of the kidney. Am. J. Physiol. Renal Physiol. 289, F200–F207. [PubMed: 15769935]

Ben Djoudi Ouadda A, Gauthier MS, Susan-Resiga D, Girard E, Essalmani R, Black M, Marcinkiewicz J, Forget D, Hamelin J, Evagelidis A, et al. (2019). Ser-phosphorylation of PCSK9 (proprotein convertase subtilisin-kexin 9) by Fam20C (family with sequence similarity 20, member C) kinase enhances its ability to degrade the LDLR (Low-Density lipoprotein receptor). Arterioscler. Thromb. Vasc. Biol. 39, 1996–2013. [PubMed: 31553664]

Benjannet S, Hamelin J, Chrétien M, and Seidah NG (2012). Loss- and gain-of-function PCSK9 variants: cleavage specificity, dominant negative effects, and low density lipoprotein receptor (LDLR) degradation. J. Biol. Chem. 287, 33745–33755. [PubMed: 22875854]

Burke AC, Dron JS, Hegele RA, and Huff MW (2017). PCSK9: regulation and target for drug development for dyslipidemia. Annu. Rev. Pharmacol. Toxicol. 57, 223–244. [PubMed: 27575716]

Chen Y-J, Ku W-C, Lin P-Y, Chou H-C, Khoo K-H, and Chen Y-J (2010). S-alkylating labeling strategy for site-specific identification of the s-nitrosoproteome. J. Proteome Res. 9, 6417–6439. [PubMed: 20925432]

Chen XW, Wang H, Bajaj K, Zhang P, Meng ZX, Ma D, Bai Y, Liu HH, Adams E, Baines A, et al. (2013). SEC24A deficiency lowers plasma cholesterol through reduced PCSK9 secretion. Elife 2, 004444–e523.

Cohen J, Pertsemlidis A, Kotowski IK, Graham R, Garcia CK, and Hobbs HH (2005). Low LDL cholesterol in individuals of African descent resulting from frequent nonsense mutations in PCSK9. Nat. Genet. 37, 161–165. [PubMed: 15654334]

Dietschy JM, and Turley SD (2002). Control of cholesterol turnover in the mouse. J. Biol. Chem. 277, 3801–3804. [PubMed: 11733542]

Dietschy JM, Turley SD, and Spady DK (1993). Role of liver in the maintenance of cholesterol and low density lipoprotein homeostasis in different animal species, including humans. J. Lipid Res. 34, 1637–1659. [PubMed: 8245716]

Emmer BT, Hesketh GG, Kotnik E, Tang VT, Lascuna PJ, Xiang J, Gingras A-C, Chen X-W, and Ginsburg D (2018). The cargo receptor SURF4 promotes the efficient cellular secretion of PCSK9. Elife 7, 388399–e38918.

Forrester MT, Foster MW, and Stamler JS (2007). Assessment and application of the biotin switch technique for examining protein S-nitrosylation under conditions of pharmacologically induced oxidative stress. J. Biol. Chem. 282, 13977–13983. [PubMed: 17376775]

Forrester MT, Thompson JW, Foster MW, Nogueira L, Moseley MA, and Stamler JS (2009). Proteomic analysis of S-nitrosylation and denitrosylation by resin-assisted capture. Nat. Biotechnol. 27, 557–559. [PubMed: 19483679]

Ge X, Zhu T, Zeng H, Yu X, Li J, Xie S, Wan J, Yang H, Huang K, and Zhang W (2021). A systematic review and meta-analysis of therapeutic efficacy and safety of alirocumab and evolocumab on familial hypercholesterolemia. BioMed Res. Int. 2021, 8032978. [PubMed: 34754882]

Goldstein JL, and Brown MS (2015). A century of cholesterol and coronaries: from plaques to genes to statins. Cell 161, 161–172. [PubMed: 25815993]

Grass DS, Saini U, Felkner RH, Wallace RE, Lago WJ, Young SG, and Swanson ME (1995). Transgenic mice expressing both human apolipoprotein B and human CETP have a lipoprotein cholesterol distribution similar to that of normolipidemic humans. J. Lipid Res. 36, 1082–1091. [PubMed: 7658156]

Hess DT, Matsumoto A, Kim S-O, Marshall HE, and Stamler JS (2005). Protein S-nitrosylation: purview and parameters. Nat. Rev. Mol. Cell Biol. 6, 150–166. [PubMed: 15688001]

Hongoh M, Haratake M, Fuchigami T, and Nakayama M (2012). A thiolmediated active membrane transport of selenium by erythroid anion exchanger 1 protein. Dalton Trans. 41, 7340–7349. [PubMed: 22580993]

Horton JD, Cohen JC, and Hobbs HH (2009). PCSK9: a convertase that coordinates LDL catabolism. J. Lipid Res. 50 (Suppl), S172–S177. [PubMed: 19020338]

Houk KN, Hietbrink BN, Bartberger MD, McCarren PR, Choi BY, Voyksner RD, Stamler JS, and Toone EJ (2003). Nitroxyl disulfides, novel intermediates in transnitrosation reactions. J. Am. Chem. Soc. 125, 6972–6976. [PubMed: 12783550]

Huang PL, Huang Z, Mashimo H, Bloch KD, Moskowitz MA, Bevan JA, and Fishman MC (1995). Hypertension in mice lacking the gene for endothelial nitric oxide synthase. Nature 377, 239–242. [PubMed: 7545787]

Huang L, Carney J, Cardona DM, and Counter CM (2014). Decreased tumorigenesis in mice with a Kras point mutation at C118. Nat. Commun. 5, 1–10.

Ignarro LJ, Buga GM, Wood KS, Byrns RE, and Chaudhuri G (1987). Endothelium-derived relaxing factor produced and released from artery and vein is nitric oxide. Proc. Natl. Acad. Sci. USA 84, 9265–9269. [PubMed: 2827174]

Jia J, Arif A, Terenzi F, Willard B, Plow EF, Hazen SL, and Fox PL (2014). Target-selective protein S-nitrosylation by sequence motif recognition. Cell 159, 623–634. [PubMed: 25417112]

Johnstone MT, Creager SJ, Scales KM, Cusco JA, Lee BK, and Creager MA (1993). Impaired endothelium-dependent vasodilation in patients with insulin-dependent diabetes mellitus. Circulation 88, 2510–2516. [PubMed: 8080489]

Kauser K, da Cunha V, Fitch R, Mallari C, and Rubanyi GM (2000). Role of endogenous nitric oxide in progression of atherosclerosis in apolipoprotein E-deficient mice. Am. J. Physiol. Heart Circ. Physiol. 278, H1679–H1685. [PubMed: 10775149]

Knowles JW, Reddick RL, Jennette JC, Shesely EG, Smithies O, and Maeda N (2000). Enhanced atherosclerosis and kidney dysfunction in eNOS(−/−)Apoe(−/−) mice are ameliorated by enalapril treatment. J. Clin. Invest. 105, 451–458. [PubMed: 10683374]

Kohr MJ, Sun J, Aponte A, Wang G, Gucek M, Murphy E, and Steenbergen C (2011). Simultaneous measurement of protein oxidation and S-nitrosylation during preconditioning and ischemia/reperfusion injury with resin-assisted capture. Circ. Res. 108, 418–426. [PubMed: 21193739]

Kornberg MD, Sen N, Hara MR, Juluri KR, Nguyen JVK, Snowman AM, Law L, Hester LD, and Snyder SH (2010). GAPDH mediates nitrosylation of nuclear proteins. Nat. Cell Biol. 12, 1094–1100. [PubMed: 20972425]

Kuhlencordt PJ, Gyurko R, Han F, Scherrer-Crosbie M, Aretz TH, Hajjar R, Picard MH, and Huang PL (2001). Accelerated atherosclerosis, aortic aneurysm formation, and ischemic heart disease in apolipoprotein E/endothelial nitric oxide synthase double-knockout mice. Circulation 104, 448–454. [PubMed: 11468208]

Lancaster JR (1994). Simulation of the diffusion and reaction of endogenously produced nitric oxide. Proc. Natl. Acad. Sci. USA 91, 8137–8141. [PubMed: 8058769]

Lane P, Hao G, and Gross SS (2001). S-nitrosylation is emerging as a specific and fundamental posttranslational protein modification: head-to-head comparison with O-phosphorylation. Sci. STKE 2001, re1.

Lee MCS, Miller EA, Goldberg J, Orci L, and Schekman R (2004). Bidirectional protein transport between the Er and golgi. Annu. Rev. Cell Dev. Biol. 20, 87–123. [PubMed: 15473836]

Li S, Yu K, Wu G, Zhang Q, Wang P, Zheng J, Liu ZX, Wang J, Gao X, and Cheng H (2021). pCysMod: prediction of multiple cysteine modifications based on deep learning framework. Front. Cell Dev. Biol. 9, 617366–617410. [PubMed: 33732693]

Marino SM, and Gladyshev VN (2010). Structural analysis of cysteine S-nitrosylation: a modified acid-based motif and the emerging role of trans-nitrosylation. J. Mol. Biol. 395, 844–859. [PubMed: 19854201]

Mayne J, Dewpura T, Raymond A, Bernier L, Cousins M, Ooi TC, Davignon J, Seidah NG, Mbikay M, and Chrétien M (2011). Novel loss-of-function PCSK9 variant is associated with low plasma LDL cholesterol in a French-Canadian family and with impaired processing and secretion in cell culture. Clin. Chem. 57, 1415–1423. [PubMed: 21813713]

Murphy E, Kohr M, Sun J, Nguyen T, and Steenbergen C (2012). S-nitrosylation: a radical way to protect the heart. J. Mol. Cell. Cardiol. 52, 568–577. [PubMed: 21907718]

Nagy P (2013). Kinetics and mechanisms of thiol-disulfide exchange covering direct substitution and thiol oxidation-mediated pathways. Antioxid. Redox Signal. 18, 1623–1641. [PubMed: 23075118]

Nakamura Y, Moss AJ, Brown MW, Kinoshita M, and Kawai C (1999). Long-term nitrate use may be deleterious in ischemic heart disease: a study using the databases from two large-scale postinfarction studies. Am. Heart J. 138, 577–585. [PubMed: 10467211]

Nakamura T, Oh CK, Liao L, Zhang X, Lopez KM, Gibbs D, Deal AK, Scott HR, Spencer B, Masliah E, et al. (2021). Noncanonical transnitrosylation network contributes to synapse loss in Alzheimer's disease. Science 371, 371. [PubMed: 33479147]

Ozaki M, Kawashima S, Yamashita T, Hirase T, Namiki M, Inoue N, Hirata KI, Yasui H, Sakurai H, Yoshida Y, et al. (2002). Overexpression of endothelial nitric oxide synthase accelerates atherosclerotic lesion formation in apoE-deficient mice. J. Clin. Invest. 110, 331–340. [PubMed: 12163452]

Palmer RM, Ferrige AG, and Moncada S (1987). Nitric oxide release accounts for the biological activity of endothelium-derived relaxing factor. Nature 327, 524–526. [PubMed: 3495737]

Pawloski JR, Hess DT, and Stamler JS (2001). Export by red blood cells of nitric oxide bioactivity. Nature 409, 622–626. [PubMed: 11214321]

Piper DE, Jackson S, Liu Q, Romanow WG, Shetterly S, Thibault ST, Shan B, and Walker NPC (2007). The crystal structure of PCSK9: a regulator of plasma LDL-cholesterol. Structure 15, 545–552. [PubMed: 17502100]

Park SW, Moon YA, and Horton JD (2004). Post-transcriptional regulation of low density lipoprotein receptor protein by proprotein convertase subtilisin/kexin type 9a in mouse liver. J. Biol. Chem. 279, 50630–50638. [PubMed: 15385538]

Seth D, Hess DT, Hausladen A, Wang L, Wang YJ, and Stamler JS (2018). A multiplex enzymatic machinery for cellular protein S-nitrosylation. Mol. Cell 69, 451–464.e6. [PubMed: 29358078]

Shankar RR, Wu Y, Shen HQ, Zhu JS, and Baron AD (2000). Mice with gene disruption of both endothelial and neuronal nitric oxide synthase exhibit insulin resistance. Diabetes 49, 684–687. [PubMed: 10905473]

Stamler JS, and Hess DT (2010). Nascent nitrosylases. Nat. Cell Biol. 12, 1024–1026. [PubMed: 20972426]

Stomberski CT, Hess DT, and Stamler JS (2019a). Protein S-nitrosylation: determinants of specificity and enzymatic regulation of S-Nitrosothiol-Based signaling. Antioxid. Redox Signal. 30, 1331–1351. [PubMed: 29130312]

Stomberski CT, Zhou H-L, Wang L, van den Akker F, and Stamler JS (2019b). Molecular recognition of S-nitrosothiol substrate by its cognate protein denitrosylase. J. Biol. Chem. 294, 1568–1578. [PubMed: 30538128]

Stomberski CT, Anand P, Venetos NM, Hausladen A, Zhou H-L, Premont RT, and Stamler JS (2019c). AKR1A1 is a novel mammalian S-nitroso-glutathione reductase. J. Biol. Chem. 294, 18285–18293. [PubMed: 31649033]

Virani SS, Alonso A, Benjamin EJ, Bittencourt MS, Callaway CW, Carson AP, Chamberlain AM, Chang AR, Cheng S, Delling FN, et al. (2020). Heart Disease and Stroke Statistics—2020 Update: A Report from the American Heart Association (American Heart Association).

Wang X, Wang H, Xu B, Huang D, Nie C, Pu L, Zajac GJM, Yan H, Zhao J, Shi F, et al. (2021). Receptor-mediated ER export of lipoproteins controls lipid homeostasis in mice and humans. Cell Metab. 33, 350–366.e7. [PubMed: 33186557]

Zhao Z, Tuakli-Wosornu Y, Lagace TA, Kinch L, Grishin NV, Horton JD, Cohen JC, and Hobbs HH (2006). Molecular characterization of loss-of-function mutations in PCSK9 and identification of a compound heterozygote. Am. J. Hum. Genet. 79, 514–523. [PubMed: 16909389]

Zhao Z, Pompey S, Dong H, Weng J, Garuti R, and Michaely P (2013). S-nitrosylation of ARH is required for LDL uptake by the LDL receptor. J. Lipid Res. 54, 1550–1559. [PubMed: 23564733]

Zhou H-L, Zhang R, Anand P, Stomberski CT, Qian Z, Hausladen A, Wang L, Rhee EP, Parikh SM, Karumanchi SA, and Stamler JS (2019). Metabolic reprogramming by the S-nitroso-CoA reductase system protects against kidney injury. Nature 565, 96–100. [PubMed: 30487609]

Highlights

- Genetic or pharmacologic inhibition of the denitrosylase SCoR2 reduces serum cholesterol
- SCoR2 functions as a COPII denitrosylase to facilitate PCSK9 export from the ER
- COPII proteins SAR1B and SURF4 act as nitrosylases to direct S-nitrosylation of PCSK9
- S-nitrosylated PCSK9 is poorly secreted, lowering serum cholesterol

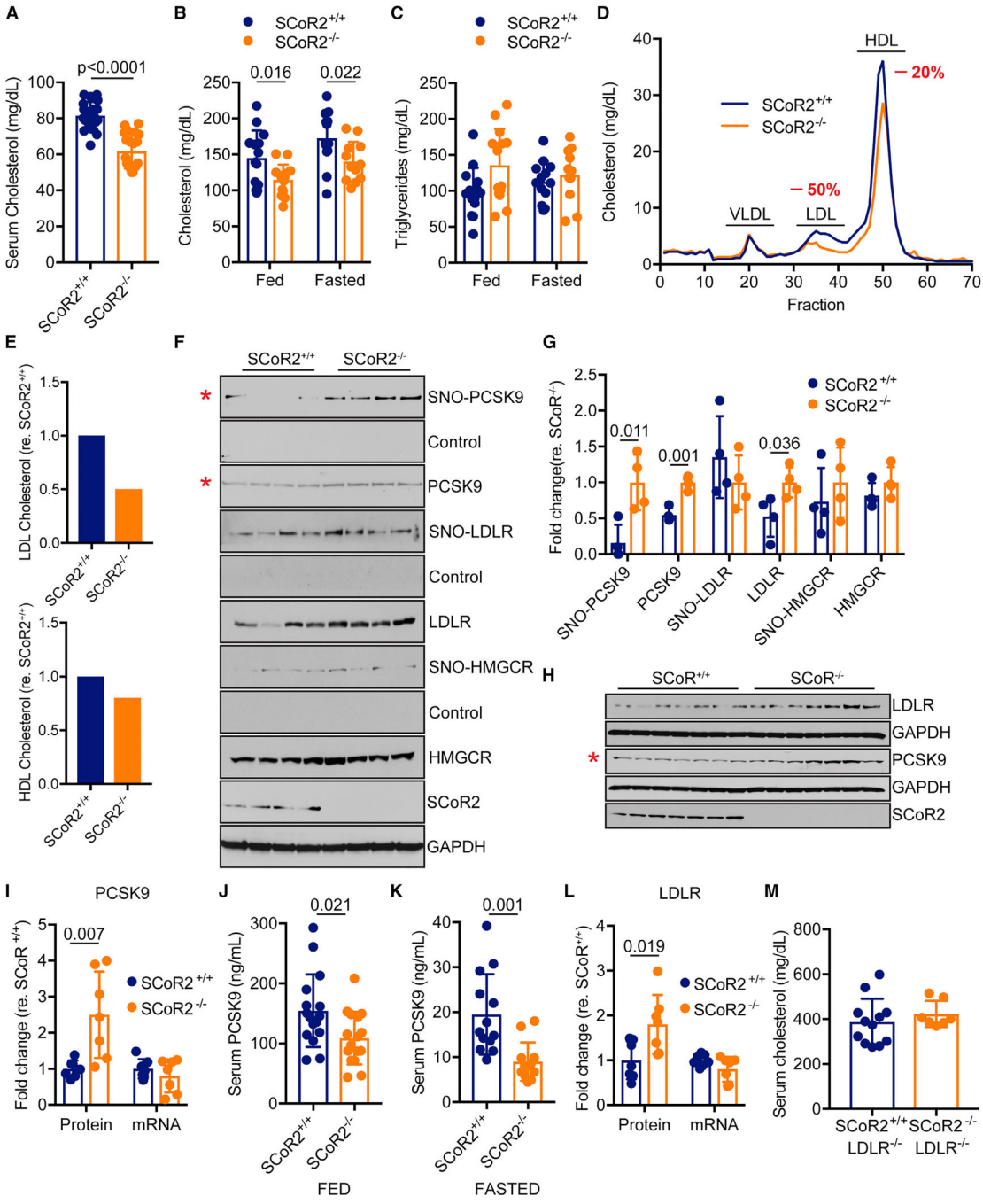

Figure 1. SCoR2$^{-/-}$ mice display LDLR-dependent hypocholesterolemia and low serum PCSK9 levels

(A) Total serum cholesterol from overnight-fasted 12-week-old male SCoR2$^{+/+}$ (n = 20) and SCoR2$^{-/-}$ mice (n = 21).

(B and C) Total serum cholesterol (B) and serum triglycerides (C) from unfasted and overnight-fasted 24-week-old male SCoR2$^{+/+}$ (n = 14 for unfasted, n = 13 for fasted) and SCoR2$^{-/-}$ mice (n = 14 for unfasted, n = 12 for fasted).

(D) Serum from 24-week-old unfasted male SCoR2$^{+/+}$ mice (n = 7) and SCoR2$^{-/-}$ mice (n = 7) were each pooled, then separated by fast protein liquid chromatography to observe lipoprotein fractions. Lipoproteins were identified compared with known standards.
(E) Graphical representation of the change in LDL (top) and HDL (bottom) cholesterol fractions from pooled samples in (D).
(F) Western blot analysis of PCSK9, LDLR, and HMGCR S-nitrosylation status (SNO) in livers from unfasted 24-week-old male SCoR2$^{+/+}$ and SCoR2$^{-/-}$ mice. *Denotes the mature, processed form of PCSK9. Control: SNO-RAC assay performed without ascorbate.
(G) Quantification (n = 4) of bands from (F). SNO-proteins were normalized to total protein for each lane and total protein was normalized to GAPDH prior to analysis. Representative SCoR2 and GAPDH blots are shown in (F).
(H) Western blot analysis for hepatic LDLR and PCSK9 from unfasted 24-week-old male SCoR2$^{+/+}$ and SCoR2$^{-/-}$ mice. *Denotes the mature, processed form of PCSK9.
(I) Quantification (n = 7) of PCSK9 protein levels from (H) and quantitative real-time PCR analysis (n = 7) of hepatic PCSK9 mRNA from the same tissue.
(J and K) Serum PCSK9 from unfasted (J) and overnight-fasted (K) 24-week-old male SCoR2$^{+/+}$ (n = 16 for unfasted, n = 13 for fasted) and SCoR2$^{-/-}$ (n = 16 for unfasted, n = 12 for fasted) mice.
(L) Quantification (n = 7) of LDLR protein levels from (H) and quantitative real-time PCR analysis (n = 7) of hepatic LDLR mRNA from the same tissue.
(M) Total serum cholesterol from unfasted 16-week-old male SCoR2$^{+/+}$/LDLR$^{-/-}$ (n = 12) and SCoR2$^{-/-}$/LDLR$^{-/-}$ mice (n = 7). See also Figures S1 and S2. In all figures, all bars represent mean ± SD, and all bands were quantified using ImageJ. p values in all figures were calculated by Student’s t test (unless noted otherwise).

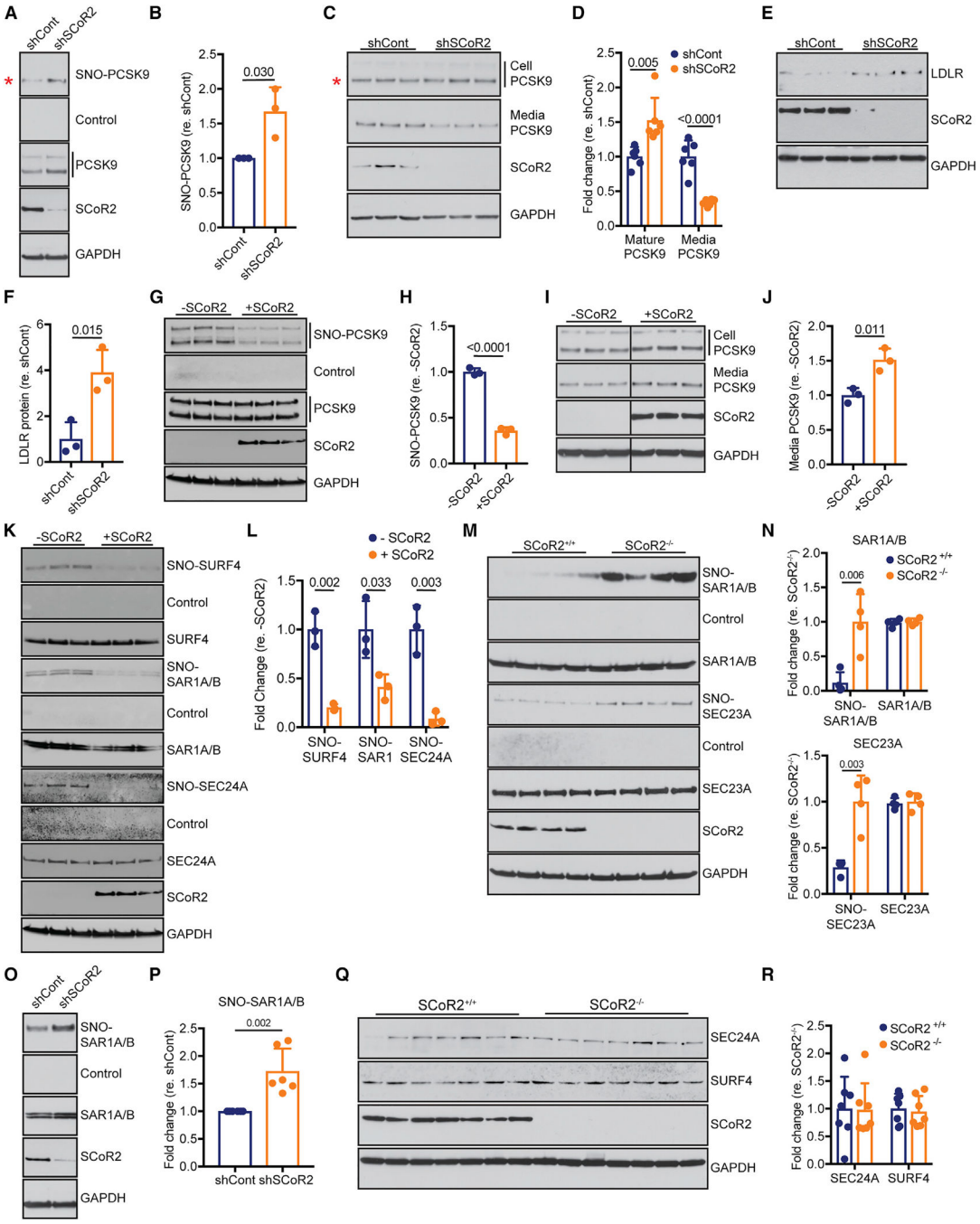

Figure 2. SCoR2 regulates S-nitrosylation of PCSK9 and its cargo-selection machinery to control secretion

(A) Western blot analysis of SNO-PCSK9 in HepG2 cells stably expressing control or SCoR2-targeting shRNA. *Denotes the mature, processed form of PCSK9.

(B) Quantification (n = 3) of SNO-PCSK9 from (A) and related experiments.

(C) Western blot analysis for cellular and secreted (media) PCSK9 in HepG2 cells stably expressing control or SCoR2-targeting shRNA. An equal number of cells were cultured for 24 h in serum-free Opti-MEM media, washed with PBS, given fresh (PCSK9-free) Opti-MEM, and harvested after 3 h. *Denotes the mature, processed form of PCSK9.

(D) Quantification (n = 6) of cellular PCSK9 (left; mature PCSK9 normalized to GAPDH input) and secreted (media) PCSK9 (right; normalized to mature PCSK9 band) from (C) and related experiments.
(E) Western blot analysis for LDLR in HepG2 cells stably expressing control or SCoR2-targeting shRNA.
(F) Quantification (n = 3) of LDLR from (E). Total LDLR was normalized to GAPDH input.
(G) Western blot analysis of SNO-PCSK9 in SCoR2-deficient HEK293 cells transiently reconstituted with SCoR2. Upper band: pro-PCSK9; lower band: mature PCSK9.
(H) Quantification (n = 3) of SNO-PCSK9 from (G).
(I) Western blot analysis for cellular and secreted (media) PCSK9 in SCoR2-deficient HEK293 cells transiently reconstituted with SCoR2. An equal number of cells were cultured for 24 h in serum-free Opti-MEM media, washed with PBS, given fresh (PCSK9-free) Opti-MEM, and harvested after 90 min. Upper band: pro-PCSK9; lower band: mature PCSK9.
(J) Quantification (n = 3) of secreted (media) PCSK9 (normalized to mature PCSK9 band) from (I).
(K) Western blot analysis of SNO-SAR1A/B, SNO-SURF4, and SNO-SEC24A in SCoR2-deficient HEK293 cells with or without reconstitution of SCoR2. V5-tagged SURF4 was overexpressed in both conditions and anti-V5 antibody used to visualize SURF4.
(L) Quantification (n = 3) of SNO-SAR1A/B (normalized to total SAR1A/B), SNO-SURF4 (normalized to total SURF4), and SNO-SEC24A (normalized to total SEC24A) from (K). Note SCoR2 and GAPDH immunoblots are shared between (G) and (K), as they are from the same experiment.
(M) Western blot analysis of SEC23A and SAR1A/B S-nitrosylation status in livers from unfasted 24-week-old $SCoR2^{+/+}$ and $SCoR2^{-/-}$ mice.
(N) Quantification (n = 4) of bands from (M). SNO-protein was normalized to total protein for each lane and total protein was normalized to GAPDH prior to analysis.
(O) Representative western blot analysis of SNO-SAR1A/B in HepG2 cells stably expressing control or SCoR2-targeting shRNA.
(P) Quantification (n = 6) of SNO-SAR1A/B (normalized to total SAR1A/B) from (O).
(Q) Western blot analysis of hepatic SEC24A and SURF4 from unfasted 24-week-old male $SCoR2^{+/+}$ and $SCoR2^{-/-}$ mice. Note, SNO-SEC24A and SNO-SURF4 were assayed but no signal was detected.
(R) Quantification (n = 7) of bands from (Q). Total target protein was normalized to GAPDH. In the above panels, SNO-proteins were captured from cell lysates by SNO-RAC, separated by SDS-PAGE, and analyzed by western blot. Control: SNO-RAC assay for SNO-proteins performed without ascorbate. See also Figure S3.

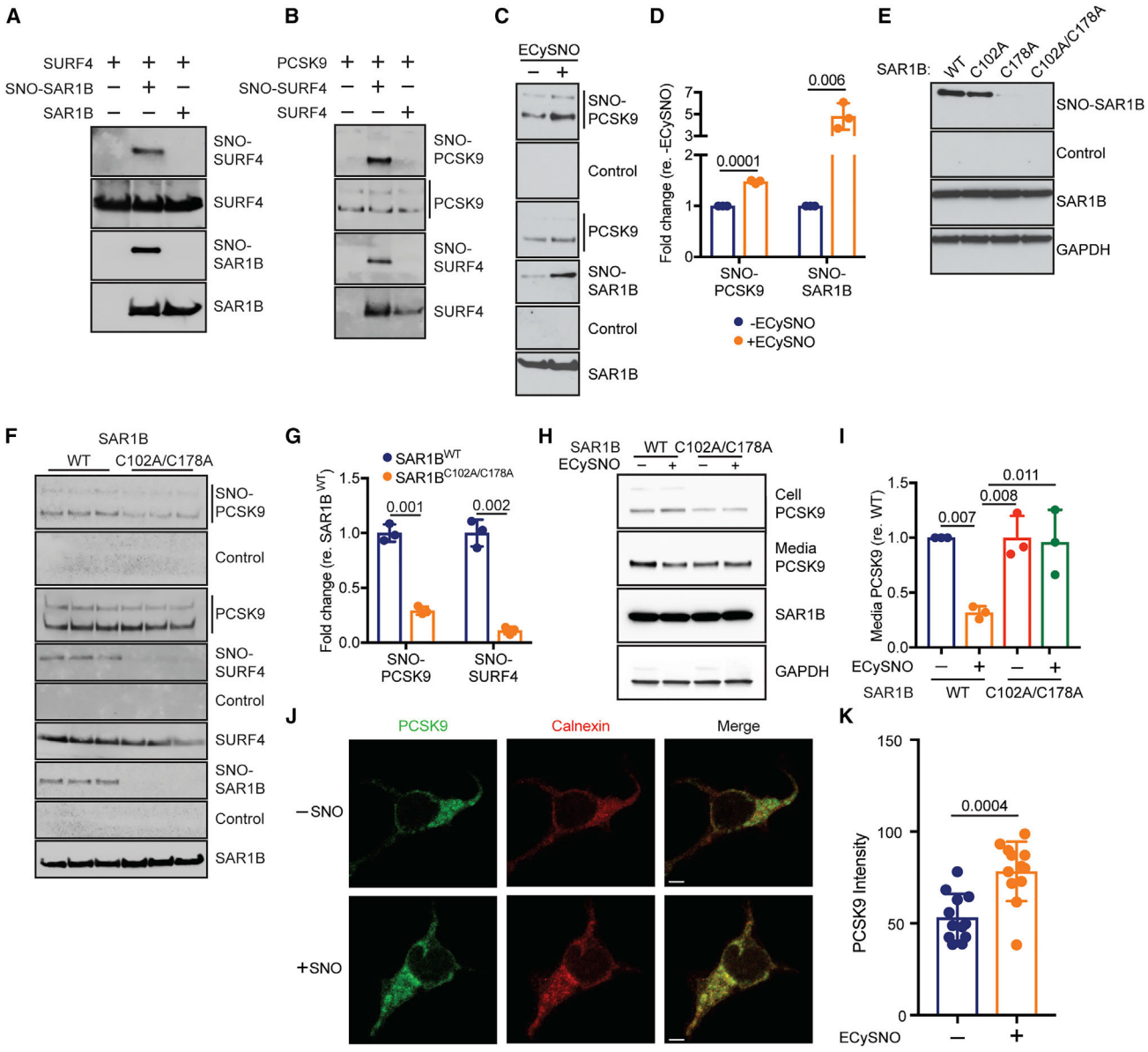

Figure 3. S-nitrosylase cascade initiated by SAR1A/B regulates PCSK9 S-nitrosylation and secretion

(A) SAR1B nitrosylates SURF4. FLAG-tagged SNO-SAR1B was incubated with V5-tagged SURF4. Reaction mixtures were subjected to SNO-RAC and SNO-proteins visualized by western blot. Representative image (n = 3) is shown.

(B) SURF4 nitrosylates PCSK9. V5-tagged SNO-SURF4 was incubated with FLAG-tagged PCSK9. Reaction mixtures were subjected to SNO-RAC and SNO-proteins visualized by western blot. Representative image (n = 3) is shown. Mature PCSK9 is visualized in SNO-PCSK9 lanes.

(C) Western blot analysis of SNO-PCSK9 and SNO-SAR1B in SCoR2-deficient HEK293 transfected with wild-type PCSK9 and wild-type SAR1B and treated with 200 μM ethyl ester S-nitroso-cysteine (ECySNO) for 90 min. Anti-FLAG antibody was used to visualize SAR1B.

(D) Quantification (n = 3) of SNO-PCSK9 and SNO-SAR1B (normalized to total PCSK9 and SAR1B, respectively) from (C) and related experiments.
(E) Western blot analysis of SNO-SAR1B wild-type and indicated mutations in SCoR2-deficient HEK293 transfected with SAR1B wild-type and indicated mutations and treated with 200 μM ECySNO for 90 min. Anti-FLAG antibody was used to visualize SAR1B in a single experiment that is verified in subsequent assays.
(F) Western blot analysis of SNO-PCSK9, SNO-SURF4, and SNO-SAR1B in SCoR2-deficient HEK293 cells transiently overexpressing $SAR1B^{WT}$ or $SAR1B^{C102A/C178A}$ and treated with 200 μM ECySNO for 90 min prior to harvest.
(G) Quantification (n = 3) of SNO-PCSK9 (mature band, normalized to total mature PCSK9) and SNO-SURF4 from (F).
(H) Representative western blot analysis for cellular and secreted (media) PCSK9 in SCoR2-deficient HEK293 cells overexpressing $SAR1B^{WT}$ or $SAR1B^{C102A/C178A}$ and treated with 200 μM ECySNO for 90 min prior to harvest.
(I) Quantification (n = 3) of secreted (media) PCSK9 (normalized to mature PCSK9 band) from (H). p values in (I) were calculated by one-way ANOVA.
(J) SCoR-deficient HEK293 cells stably expressing PCSK9 were treated with or without 200 μM ECySNO (+SNO) for 90 min then stained with anti-PCSK9 (green) and anti-calnexin (red, ER marker) antibodies. Scale bar, 5 μm.
(K) Quantification of mean PCSK9 signal intensity in pixels positive for calnexin (n = 12 cells per condition). Control: SNO-RAC assay performed without ascorbate. See also Figure S4.

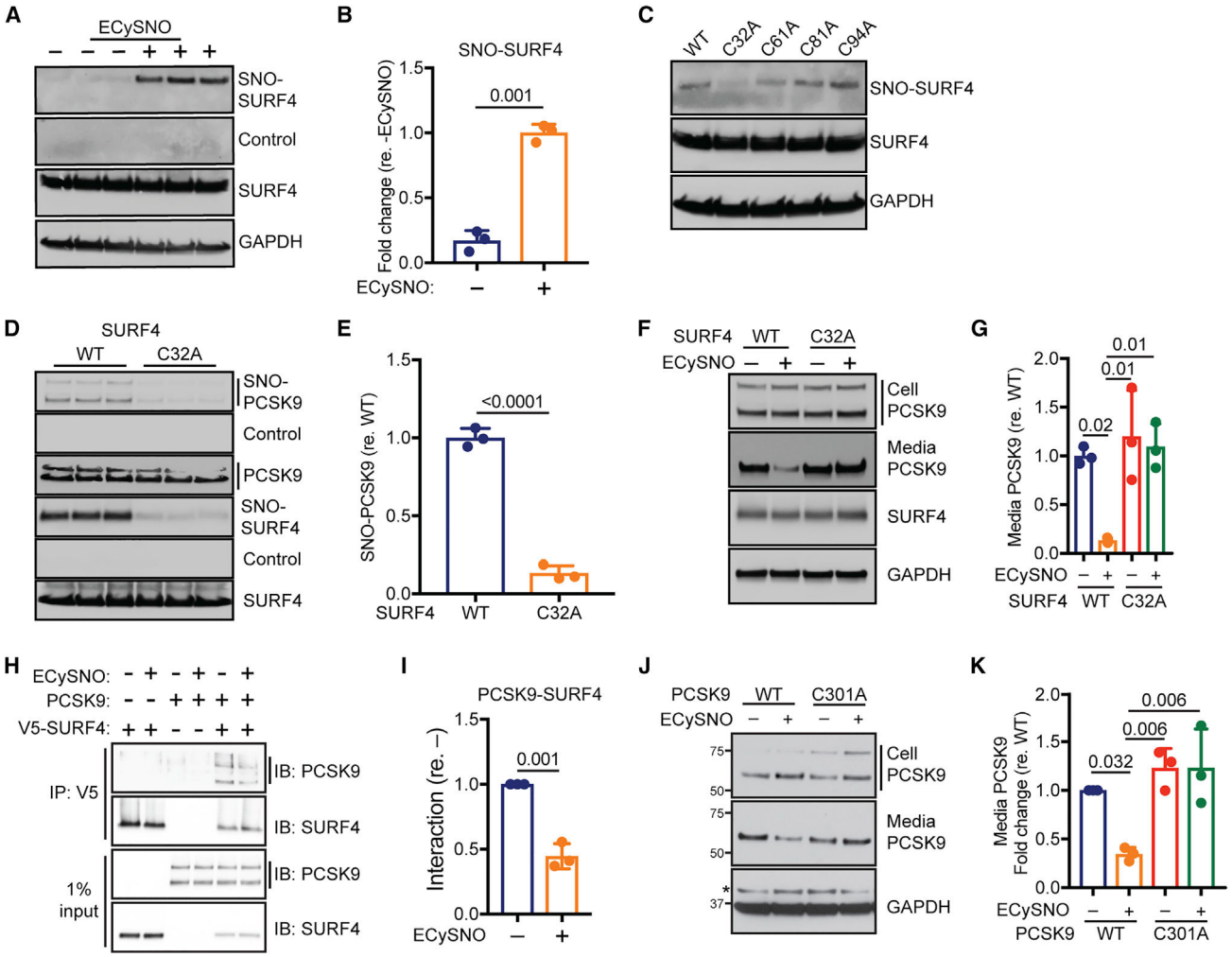

Figure 4. SURF4 S-nitrosylates PCSK9 to inhibit cargo selection and secretion

(A) Western blot analysis of SNO-SURF4 in SCoR2-deficient HEK293 transfected with wild-type SURF4 and treated with 200μM ECySNO for 90 min. Anti-V5 antibody was used to visualize SURF4.

(B) Quantification (n = 3) of SNO-SURF4 (normalized to total SURF4) from (A).

(C) Western blot analysis of SNO-SURF4 in SCoR2-deficient HEK293 transfected with SURF4 wild-type or indicated mutants and treated with 200 μM ECySNO for 90 min. Anti-V5 antibody was used to visualize SURF4 in a single experiment that is verified in subsequent assays.

(D) Western blot analysis of SNO-PCSK9 and SNO-SURF4 in SCoR2-deficient HEK293 cells transiently overexpressing $SURF4^{WT}$ or $SURF^{C32A}$ and treated with 200 μM ECySNO for 90 min prior to harvest.

(E) Quantification (n = 3) of SNO-PCSK9 (mature band, normalized to total mature PCSK9) from (D).

(F) Western blot analysis for cellular and secreted (media) PCSK9 in SCoR2-deficient HEK293 cells overexpressing $SURF4^{WT}$ or $SURF4^{C32A}$ and treated with 200 μM ECySNO for 90 min prior to harvest.

(G) Quantification (n = 3) of secreted (media) PCSK9 (normalized to mature PCSK9 band) from (F).

(H) Western blot analysis of PCSK9–SURF4 interaction with or without ECySNO treatment. An equal number of cells were transfected and cultured for 24 h, washed with PBS, given fresh (PCSK9-free) Opti-MEM media with or without 200 μM ECySNO, and harvested after 20 min. SURF4 was visualized with anti-V5 antibody.

(I) Quantification (n = 3) of PCSK9–SURF4 interaction with or without ECySNO treatment from (H).

(J) Western blot analysis of cellular and secreted (media) PCSK9 in SCoR2-deficient HEK293 transiently expressing $PCSK9^{WT}$ or $PCSK9^{C301A}$ with or without ECySNO treatment. An equal number of cells were transfected and cultured for 24 h, washed with PBS, given fresh (PCSK9-free) Opti-MEM media with or without 200 μM ECySNO, and harvested after 90 min.

(K) Quantification (n = 3) of secreted (media) PCSK9 (normalized to mature PCSK9, lower band) from (J) and related experiments. p values in (G) and (K) were calculated by one-way ANOVA. In the above panels, SNO-proteins were captured from cell lysates by SNO-RAC, separated by SDS-PAGE, and analyzed by western blot. Control; SNO-RAC assay for SNO-proteins performed without ascorbate. For PCSK9, upper band: pro-PCSK9; lower band: mature PCSK9. See also Figure S6

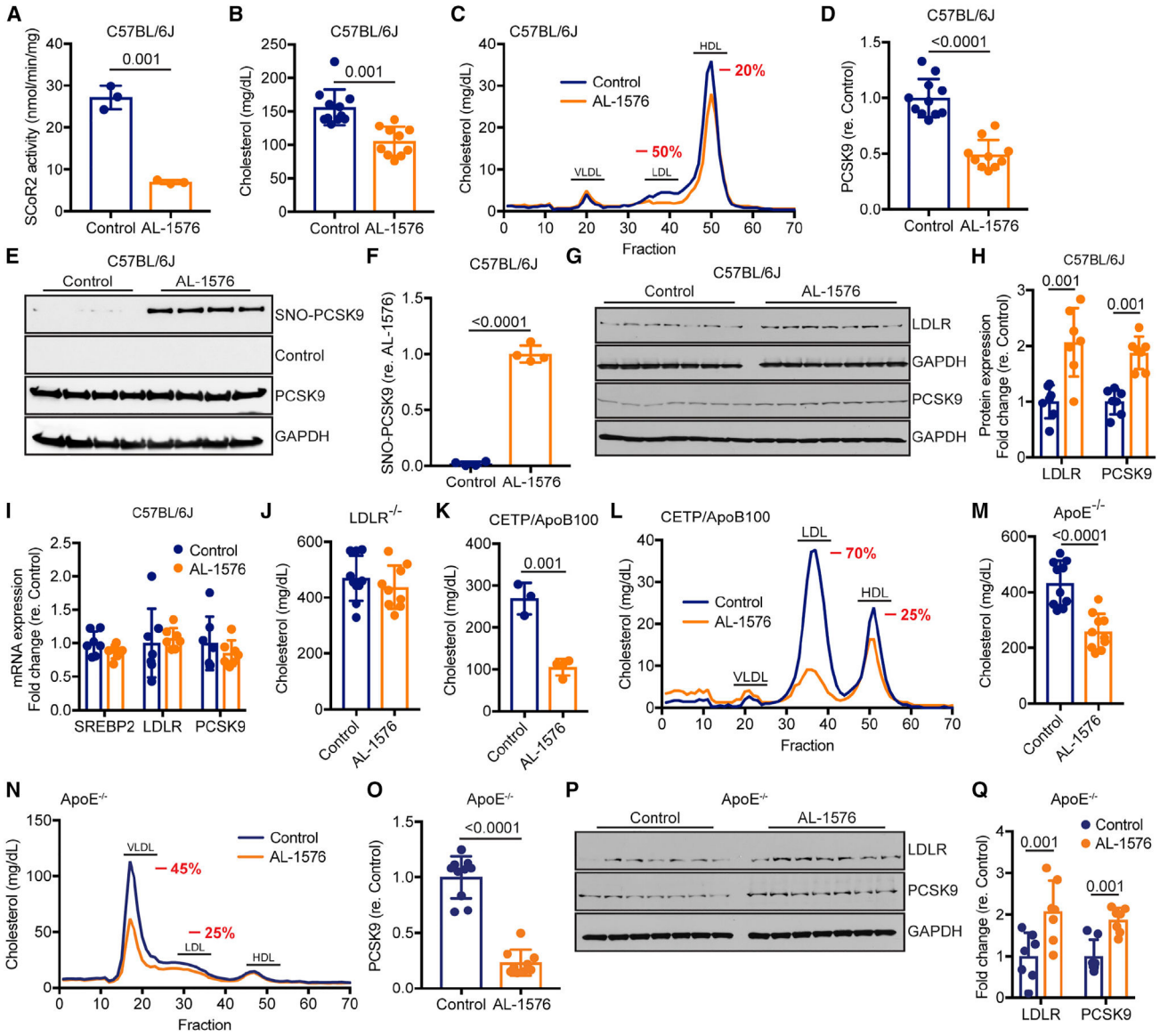

Figure 5. Inhibition of SCoR2 by small-molecule drug increases SNO-PCSK9 levels and lowers serum LDL cholesterol

(A) SNO-CoA reductase activity in liver lysate from control-fed C57BL/6J mice or mice fed diet containing AL-1576 for 4 weeks (n = 3).

(B) Total serum cholesterol from 6-h fasted 20-week old male mice fed control diet (n = 10) or fed diet containing AL-1576 for 4 weeks (n = 10).

(C) Pooled serum from 6-h fasted 20-week-old male mice fed control diet (n = 7) or fed diet containing AL-1576 for 4 weeks (n = 7) was separated by fast protein liquid chromatography to obtain individual lipoprotein fractions. Lipoprotein fractions were labeled according to known standards.

(D) Serum PCSK9 from 6-h fasted 20-week-old male mice fed control diet (n = 10) or fed diet containing AL-1576 for 4 weeks (n = 10).

(E) Western blot analysis of SNO-PCSK9 in livers from 6-h fasted 20-week-old male mice fed control diet (n = 4) or fed diet containing AL-1576 for 4 weeks (n = 4). Control; SNO-RAC assay for SNO-PCSK9 performed without ascorbate. Mature PCSK9 is visualized.
(F) Quantification (n = 4) of bands from (E). SNO-protein was normalized to total protein for each lane and total protein was normalized to GAPDH prior to analysis.
(G) Western blot analysis for hepatic LDLR and PCSK9 from 6-h fasted 20-week-old mice fed control diet or fed diet containing AL-1576 for 4 weeks. Mature PCSK9 is visualized.
(H) Quantification (n = 7) of LDLR and PCSK9 protein levels from (G).
(I) Quantitative real-time PCR analysis of hepatic SREBP2, LDLR, and PCSK9 from 6-h fasted 20-week-old mice fed control diet (n = 7) or fed diet containing AL-1576 for 4 weeks (n = 7).
(J) Total serum cholesterol from 6-h fasted 16-week-old male $LDLR^{-/-}$ mice (n = 10) or $LDLR^{-/-}$ mice fed diet containing AL-1576 for 4 weeks (n = 9).
(K) Total serum cholesterol from 6-h fasted 16-week-old male CETP/ApoB100 transgenic mice fed control diet (n = 3) or fed diet containing AL-1576 for 8 weeks (n = 4).
(L) Pooled serum from 6-h fasted 16-week-old male CETP/ApoB100 transgenic mice fed control diet (n = 3) or fed diet containing AL-1576 for 8 weeks (n = 4) was separated by fast protein liquid chromatography to obtain individual lipoprotein fractions. Lipoprotein fractions were labeled according to known standards.
(M) Total serum cholesterol from 6-h fasted 20-week-old male $ApoE^{-/-}$ mice fed control diet (n = 10) or fed diet containing AL-1576 for 4 weeks (n = 10).
(N) Serum from 6-h fasted 20-week-old male $ApoE^{-/-}$ mice fed control diet (n = 10) or diet containing AL-1576 for 4 weeks (n = 10) was separated by fast protein liquid chromatography to obtain individual lipoprotein fractions. Lipoprotein fractions were labeled according to known standards.
(O) Serum PCSK9 from 6-h fasted 20-week-old male $ApoE^{-/-}$ mice fed control diet (n = 10) or diet containing AL-1576 for 4 weeks (n = 10).
(P) Western blot analysis for hepatic LDLR and PCSK9 from 6-h fasted 20-week-old $ApoE^{-/-}$ mice fed control diet or diet containing AL-1576 for 4 weeks.
(Q) Quantification (n = 7) of LDLR and PCSK9 protein levels from (P).

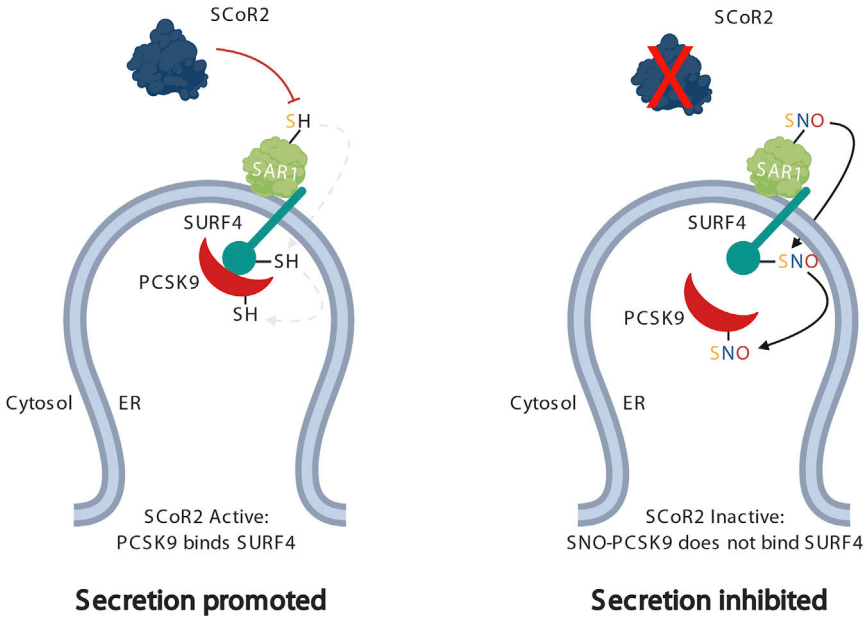

Figure 6. SCoR2 regulates S-nitrosylation of COPII proteins to control PCSK9 S-nitrosylation and secretion

(Left) SCoR2 enables PCSK9 secretion by preventing S-nitrosylation of COPII components (SAR1, and SURF4) and cargo (PCSK9). PCSK9 can bind its cargo receptor SURF4 to promote selection of PCSK9 into nascent ER vesicles. (Right) SCoR2 inhibition (genetically or pharmacologically) blocks PCSK9 secretion via an S-nitrosylation cascade thereby lowering LDL cholesterol. Specifically, inhibition of SCoR2 leads to increases in SAR1 S-nitrosylation; SNO-SAR1 then acts as a nitrosylase for SURF4 to form SNO-SURF4, which then nitrosylates PCSK9 to inhibit PCSK9-SURF4 interaction. That is, SNO-PCSK9 binding to SURF4 is ineffectual, preventing selection of PCSK9 into nascent ER vesicles, thereby reducing PCSK9 secretion. Created with BioRender.com.

KEY RESOURCES TABLE

REAGENT or RESOURCE	SOURCE	IDENTIFIER
Antibodies		
Mouse monoclonal SCoR/AKR1A1	Santa Cruz Biotechnology	sc-100500 RRID:AB_118799
Rabbit polyclonal GAPDH	Proteintech	10494-1-AP RRID:AB_2263076
Rabbit monoclonal LDLR	Abcam	ab52818 RRID:AB_881213
Goat polyclonal mouse PCSK9	R&D Systems	AF3985 RRID:AB_2044717
Rabbit monoclonal human PCSK9	Cell Signaling	85,813 RRID:AB_2800064
Rabbit polyclonal PCSK9	Proteintech	55206-1-AP RRID:AB_10918272
Rabbit monoclonal HMGCR	Abcam	ab174830 RRID:AB_2749818
Rabbit polyclonal ACAT2	Cell Signaling	11,814
Rabbit polyclonal ARH	Proteintech	13213-1-AP RRID:AB_2135283
Rabbit monoclonal SAR1A/B	Abcam	ab155278
Rabbit polyclonal SEC23A	Cell Signaling	8162 RRID:AB_10859891
Goat polyclonal SEC23A	Novus Biologicals	NBP1-47201 RRID:AB_10010164
Rabbit polyclonal SEC24A	Proteintech	15958-1-AP RRID:AB_2186118
Rabbit polyclonal SURF4	Sigma-Aldrich	SAB2108065
Rabbit monoclonal V5	Cell Signaling	13,202 RRID:AB_2687461
Mouse monoclonal calnexin	Proteintech	66903-1-Ig RRID:AB_2882231
Goat polyclonal rabbit IgG Alexa Fluor 488	Thermo Fisher	A-11008 RRID:AB_143165
Goat polyclonal mouse IgG Alexa Fluor 594	Thermo Fisher	A-11005 RRID:AB_2534073
Donkey polyclonal rabbit IgG Alexa Fluor 488	Thermo Fisher	A-32790 RRID:AB_2762833
Donkey polyclonal goat IgG Alexa Fluor 594	Thermo Fisher	A-11058 RRID:AB_142540
Chemicals, peptides, and recombinant proteins		
Sodium ascorbate	Sigma-Aldrich	Cat #11140
S-methyl thiomethansulfonate, MMTS	Sigma-Aldrich	Cat #64306
Thiopropyl Sepharose 6B	GE Lifesciences	Cat #17-0420-01
Cysteine ethyl ester hydrochloride	Sigma-Aldrich	Cat #C121908
Coenzyme A	Sigma-Aldrich	Cat #C4780
Cysteine	Sigma-Aldrich	Cat #C6852
V5 affinity agarose	Sigma-Aldrich	Cat #A7345
V5 peptide	Sigma-Aldrich	Cat #V7754
FLAG affinity agarose	Sigma-Aldrich	Cat #A2220
FLAG peptide	Sigma-Aldrich	Cat #F3290
3X FLAG peptide	Sigma-Aldrich	Cat #F4799
IodoTMT	Thermo Fisher	Cat #90101
Iodoacetamide	Sigma-Aldrich	Cat #I1149
Anti-TMT resin	Thermo Fisher	Cat #90076
AL-1576	TCG Lifesciences, WuXi China	Custom synthesis

REAGENT or RESOURCE	SOURCE	IDENTIFIER
Critical commercial assays		
High capacity RNA-to-cDNA kit	Applied Biosystems	Cat #4387406
TaqMan University Master Mix II (without UNG)	Thermo Fisher	Cat #4440043
LDLR TaqMan Probe	Thermo Fisher	Cat # Mm01177349_m1
PCSK9 TaqMan Probe	Thermo Fisher	Cat # Mm0126310_m1
SREBF2 TaqMan Probe	Thermo Fisher	Cat # Mm01306292_m1
GAPDH TaqMan Probe	Thermo Fisher	Cat # Mm99999915_g1
Cholesterol Assay	Abcam	Cat #ab65359
Triglyceride Assay	Cayman Chemicals	Cat #10010303
Mouse PCSK9 ELISA	R&D Systems	Cat #MPC900
Mouse alpha-1-antitrypsin ELISA	Crystal Chem	Cat #80631
Deposited data		
Blot and image raw files	Mendeley Data	https://doi.org/10.17632/z2fm5g6tcf
Experimental models: Cell lines		
Human: HepG2 stably expressing non-targeting shRNA	This study	N/A
Human: HepG2 stably expressing SCoR-targeting shRNA	This study	N/A
Human: 293T/17	ATCC	Cat #CRL-11268 RRID:CVCL_1926
Human: SCoR-deficient HEK293	Stomberski et al., (2019a)	PMID:30538128
Human: SCoR-deficient HEK293 stably expressing PCSK9	This study	N/A
Experimental models: Organisms/strains		
Mouse: AKR1A1^{tm1Dgen}	Deltagen	N/A
Mouse: C57BL/6J	The Jackson Laboratory	Strain #000664 RRID:IMSR_JAX:000,664
Mouse: B6.129S7-Ldlr^{tm1Her}/J	The Jackson Laboratory	Strain #002207 RRID:IMSR_JAX:002,207
Mouse: B6.SJL-Tg(APOA-CETP) 1dsgTg(APOB100)1102SgyN10	Taconic	Strain #3716-M RRID:IMSR_TAC:3716
Mouse: B6.129P2-Apoe^{tm1Unc}/J	The Jackson Laboratory	Strain #002052 RRID:IMSR_JAX:002,052
Mouse: AKR1A1$^{-/-}$/LDLR$^{-/-}$	This Study	N/A
Oligonucleotides		
Mouse Genotyping Primers: See Table S1	This Study	N/A
PCSK9, SURF4, SAR1B mutagenesis primers: See Table S2	This Study	N/A
Mammalian non-targeting shRNA	Sigma-Aldrich	Cat #SHC002
SCoR-targeting shRNA	Sigma-Aldrich	Cat # TRCN0000231969
Recombinant DNA		
pEntr223.1-PCSK9	Dharmacon	Cat #OHS5893-202503467
pEntr223.1-PCSK9-Fusion	DNASU	Cat # HsCD00294884
pCSF107mT-GATEWAY-3′-FLAG	Todd Stukenberg Lab	Addgene Cat #67619
pcDNA-Dest40	Thermo Fisher	Cat #12274015

REAGENT or RESOURCE	SOURCE	IDENTIFIER
pcDNA-Dest40-PCSK9^{WT}	This Study	N/A
pcDNA-Dest40-PCSK9^{C301A}	This Study	N/A
pCSF107mT-PCSK9-3′-FLAG	This Study	N/A
pDONR221-SURF4	DNASU	Cat # HsCD00044097
pcDNA3.2/nV5-DEST	Thermo Fisher	Cat #12290010
pcDNA3.2/nV5-SURF4^{WT}	This Study	N/A
pcDNA3.2/nV5-SURF4^{C32A}	This Study	N/A
pCMV6-SAR1B^{WT}	Origene	Cat #RC213692
pCMV6-SAR1B$^{C102A/C178A}$	This Study	N/A
pCMV6-AKR1A1^{WT}	Origene	Cat #RC200302
Software and algorithms		
GraphPad Prism v7	GraphPad Inc	N/A
Other		
Mouse Diet: AIN-93M + 1% ascorbic acid	Research Diets	Cat #D16021012, custom diet
Mouse Diet: AIN-93M + 0.0125% AL-1576	Research Diets	Cat #D15111101, custom diet
Mouse Diet: AIN-93M	Research Diets	Cat #D10012M